Spring 2024

UPA-Mediated Polyamidoamine Dendrimer-Based Targeted Gene Delivery System on Triple-Negative Breast Cancer

Hsin-Yin Chuang
Missouri University of Science and Technology

Department:

uPA-MEDIATED POLYAMIDOAMINE DENDRIMER-BASED TARGETED GENE DELIVERY SYSTEM ON TRIPLE-NEGATIVE BREAST CANCER

by

HSIN-YIN CHUANG

A THESIS

Presented to the Graduate Faculty of the

MISSOURI UNIVERSITY OF SCIENCE AND TECHNOLOGY

In Partial Fulfillment of the Requirements for the Degree

MASTER OF SCIENCE

in

BIOLOGICAL SCIENCES

2023

Approved by:

Yue-Wern Huang, Advisor
Hu Yang, Co-advisor
Katie Shannon
Anthony Convertine

PUBLICATION THESIS OPTION

This thesis consists of the following one article, formatted in the style used by the Missouri University of Science and Technology:

Paper I: Pages 6-55 are intended for submission to *Journal of Controlled Release*.

ABSTRACT

Around 15% of breast cancers are triple-negative breast cancer (TNBC), which is characterized by the absence of three common receptors—ER, PR, and HER2, and therefore do not respond to hormonal or anti-HER2 therapies. It is urgent to explore targeted therapeutic strategies for TNBC due to its poor prognosis and rare effective targeted therapy. In this study, we developed a polyamidoamine (PAMAM) dendrimer-based targeted gene delivery system—GDP-uPA, to utilize urokinase-type plasminogen activator (uPA) to target uPA receptor (uPAR), which is highly expressed in both TNBC cells and cancer-associated stromal cells. Our results of ^{1}H NMR spectrum, TEM imaging, and MTT assay showed characterization of functionalized dendrimers (16.45 nm) and their high biocompatibility (25 μg/ml) in MDA-MB-231 TNBC cell line. Results of flow cytometer and confocal microscopy showed that GDP-uPA improved the delivery of GTI-2040 (GTI), an anticancer oligonucleotide, in MDA-MB-231 cell line and HCC2218 fibroblast cell line up to 6-fold compared to the GTI only group. GDP-uPA/GTI killed cells by ~30% through knock-downing human ribonucleotide reductase component (R2) by 35%. In addition, biodistribution and therapeutic studies showed a significant inhibition of tumor growth in the TNBC orthotopic xenograft mice model with GDP-uPA/GTI administration for 14 days. Collectively, GDP-uPA improved the transfection efficiency of anticancer nucleic acids in both breast cancer cells and cancer-associated stromal cells, showing the targeted capacity and attenuated tumor growth in mice model. GDP-uPA has great potential in developing efficient targeted delivery systems to treat TNBC.

ACKNOWLEDGMENTS

I would like to express my gratitude to my co-advisors, Dr. Yue-Wern Huang and Dr. Hu Yang. Without their support and guidance, it would not have been possible for me to complete this thesis and receive the John W. Claypool Medical Research Fund and Graduate Research Presentation Award in 2023. I am grateful for their time and dedication during my graduate studies in S&T, which resulted in some incredible experiences and opportunities, including working with different groups and projects and attending international conferences. I would like to thank Dr. Katie Shannon and Dr. Anthony Convertine for serving on my committee and giving me advice on my research. I am grateful to my previous advisor, Dr. Hsiu-Mei Hsieh of National Taiwan Normal University, for encouraging me to pursue this degree and broaden my horizons in the United States.

In addition, I would like to thank Dr. Yang's lab members, especially Anna Chernatynskaya, Dr. Da Huang, Lin Qi, Vidit Singh, and Dr. Vimalin Jeyalatha Mani, for their professional assistance and strong backup. I have learned many new techniques and acquired comforts from them. I would also thank Richard J. Watters for *in vivo* experiment training.

Last but not least, I sincerely thank my family in Taiwan and appreciate their love, patience, and support.

TABLE OF CONTENTS

Page

LIST OF ILLUSTRATIONS

SECTION Page

LIST OF TABLES

SECTION Page

1. INTRODUCTION

Breast cancer is the most prevalent cancer (31%) among women in the United States.[1-3] Analysis of breast tumors using immunohistochemistry to determine the expression of estrogen receptor (ER), progesterone receptor (PR), and human epidermal growth factor receptor 2 (HER2) is a widely accepted method in clinical settings and can help make better treatment decisions.[4-6] Based on these molecular characteristics, breast cancer can be generally categorized into the following five subtypes: i) Luminal A (ER+, PR+, and HER2−); ii) Luminal B (ER+,PR+/− and HER2+/−); iii) HER2-positive (ER−, PR−, and HER2+); iv) Triple-negative (TNBC) or basal-like (ER−, PR−, and HER2−); v) Other special subtypes.[4, 7-12] It is well known that patients with different subtypes of breast cancers have different prognosis and need different treatments,[13, 14] as shown in Table 1.1.

Additionally, numerous prognostic factors are related to poor survival of breast cancer patients, such as late tumor detection, advanced-stage caner, larger tumor size, higher-grade tumor, more lymph node involvement, receptor status and molecular subtypes, and occurrence of recurrence and metastasis.[15-18] Breast cancer treatments should be tailored to different molecular signatures, receptor expressions, and cancer stages to improve treatment effectiveness. Based on these differences, breast cancer patients may undergo various forms of treatment, including surgery, radiation therapy, chemotherapy, hormonal therapy, and targeted therapy, as shown in Table 1.1.[19, 20] Targeted therapies for breast cancer have come a long way over the past 25 years. Figure 1.1 summarizes a timeline of breast cancer targeted therapy drug classes, organized by year of U.S. Federal Drug Administration (FDA) approval.[21]

Table 1.1 Classification of molecular subtypes of breast cancer and therapies.

Molecular Subtypes	Luminal A	Luminal B		HER2+	TNBC
		HER2−	HER2+		
Biomarkers	ER+ PR+ HER2−	ER+ PR− HER2−	ER+ PR+/− HER2+	ER− PR− HER2+	ER− PR− HER2−
Frequency Cases (%)	50	15		20	15
Histological Grade	Well differentiated (Grade I)	Moderately differentiated (Grade II)		Little differentiated (Grade III)	Little differentiated (Grade III)
Prognosis	Good	Intermediate		Poor	Poor
Response to Therapies	Endocrine Chemotherapy	Endocrine, Chemotherapy	Endocrine, Chemotherapy, Anti-HER2 therapy	Anti-HER2 therapy, Chemotherapy	Chemotherapy, PARP inhibitors, Immunotherapy

ER: estrogen receptor; PR: progesterone receptor; HER2: human epidermal growth factor receptor 2. Endocrine therapy includes tamoxifen, letrozole, anastrozole, and exemestane. Chemotherapy includes adriamycin/cyclophosphamide (AC), AC/paclitaxel (AC-T), and docetaxel/cyclophosphamide (TC). Anti-HER2 therapy: trastuzumab or pertuzumab. The table is modified and derived from three review papers.[4, 25, 26]

Around 15% of breast cancers are triple-negative breast cancer (TNBC), which is the most aggressive subtype and characterized by the absence of three common receptors—ER, PR, and HER2.[8-12] Epidemiological studies show that TNBC mostly occurs in premenopausal women under the age of 40.[22, 23] TNBC patients generally have shorter survival compared with other breast cancer subtypes, with a mortality rate of 40% within the first 5 years after diagnosis.[24] TNBC is known for its highly aggressive nature, with more than one-third of TNBC patients will develop distant metastases.[24, 27-29]

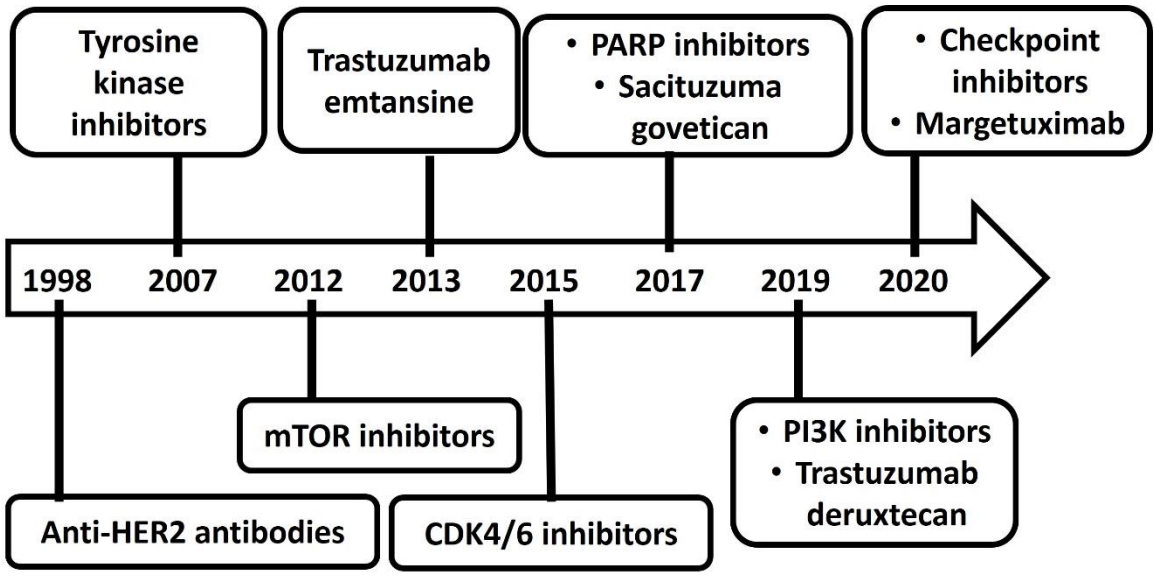

Figure 1.1. Timeline of US Federal Drug Administration approval of targeted therapy drug classes/drugs for breast cancer. The figure was remade and derived from the review parper.[21]

Due to its special molecular phenotype, TNBC does not respond to endocrine therapy or anti-HER2 targeted therapy (Table 1.1). Chemotherapy has been the main treatment for TNBC for a long time; however, there have been recent developments in the treatment landscape. This includes the introduction of poly(ADP-ribose) polymerase inhibitors (PARPis) for patients with BRCA mutations (BRCAmut) and the combination of immunotherapy and chemotherapy in tumors showing PD-L1 positivity (at least 1% of PD-L1 expression in tumor-infiltrating immune cells).[30-33] These targeted therapies improve overall survival of patients, whereas have shown incidence of adverse events,[34] can be resistant by tumor cells, and are not suitable for patients without BRCAmut or PD-L1.[30-33, 35] Overall, it is urgently needed to develop a novel therapy to improve treatment success in TNBC due to its poor prognosis and rare effective targeted therapy.

Recently, the focus of TNBC treatment has been on nanocarriers for drug delivery system to achieve enhanced availability, targeted cellular uptake, and minimal toxicity.[36] These nanocarriers, such as liposomes, micelles, dendrimers, and polymeric nanoparticles, carry all the necessary components (drugs, targeted ligands, tracking probes) and are designed in a way to specifically target the TNBC cells in the field.[37] Most of these nano delivery systems for TNBC rely on the enhanced permeation and retention (EPR) effect[38] and receptor-ligand-mediated active targeting for targeted drug delivery. Most targeted delivery approaches utilize the corresponding ligands of the receptor that are highly expressed in TNBC, like epidermal growth factor receptor (EGFR)[39] and cluster-determinant 44 receptor (CD44)[40], to as targeted ligands. The use of nanotechnology for drug delivery, combined with comprehensive systems of complementary components such as drugs, ligands, and probes, has the potential to improve diagnostic accuracy and therapeutic efficacy, and further enhance patient survival and life quality.[36, 37]

In this thesis, we developed a polyamidoamine (PAMAM) dendrimer-based [41-44] targeted gene delivery system—GDP-uPA, to utilize urokinase-type plasminogen activator (uPA) to target uPA receptor (uPAR),[45-50] which is highly expressed in both TNBC cells and cancer-associated stromal cells.[51-53] The GDP-uPA was evaluated for its ability to target cancer and its microenvironment and improve the transfection efficiency of an anticancer nucleic acid GTI-2040 (GTI).

In summary, GDP-uPA improved the transfection efficiency of anticancer nucleic acids in both breast cancer cells and cancer-associated stromal cells, showing the targeted capacity and attenuated tumor growth in mice model. GDP-uPA has great potential in developing efficient targeted delivery systems to treat TNBC.

PAPER

I. uPA-MEDIATED POLYAMIDOAMINE DENDRIMER-BASED TARGETED GENE DELIVERY SYSTEM ON TRIPLE-NEGATIVE BREAST CANCER

ABSTRACT

Around 15% of breast cancers are triple-negative breast cancer (TNBC), which is characterized by the absence of three common receptors—ER, PR, and HER2, and therefore do not respond to hormonal or anti-HER2 therapies. It is urgent to explore targeted therapeutic strategies for TNBC due to its poor prognosis and rare effective targeted therapy. In this study, we developed a polyamidoamine (PAMAM) dendrimer-based targeted gene delivery system—GDP-uPA, to utilize urokinase-type plasminogen activator (uPA) to target uPA receptor (uPAR), which is highly expressed in both TNBC cells and cancer-associated stromal cells. The GDP-uPA was evaluated for its ability to target cancer and its microenvironment and improve the transfection efficiency of anticancer nucleic acid. Our results of ^{1}H NMR spectrum, TEM imaging, and MTT assay showed characterization of functionalized dendrimers (16.45 nm) and their high biocompatibility (25 μg/ml) in MDA-MB-231 TNBC cell line. Results of flow cytometer and confocal microscopy showed that GDP-uPA improved the delivery of GTI-2040 (GTI), an anticancer oligonucleotide, in MDA-MB-231 cell line and HCC2218 fibroblast cell line up to 6-fold compared to the GTI only group. GDP-uPA carrying GTI (GDP-uPA/GTI) killed cells by ~30% through knock-downing human ribonucleotide reductase component (R2) by 35%. In addition, biodistribution and therapeutic studies showed a

significant inhibition of tumor growth in the TNBC orthotopic xenograft mice model with GDP-uPA/GTI administration for 14 days. Collectively, GDP-uPA improved the transfection efficiency of anticancer nucleic acids in both breast cancer cells and cancer-associated stromal cells, showing the targeted capacity and attenuated tumor growth in mice model. GDP-uPA has great potential in developing efficient targeted delivery systems to treat TNBC.

Keywords: targeted gene delivery, antisense oligonucleotide, urokinase-type plasminogen activator receptor (uPAR), polyamidoamine (PAMAM) dendrimer, triple-negative breast cancer (TNBC)

1. INTRODUCTION

Breast cancer is the most prevalent cancer among women in the United States.[1-3] Around 15% of breast cancers are triple-negative breast cancer (TNBC), which is the most aggressive subtype and characterized by the absence of three common receptors—estrogen receptor (ER), progesterone receptor (PR), and human epidermal growth factor receptor 2 (HER2),[4-8] and therefore do not respond to hormonal or anti-HER2 therapies. Conventional chemotherapies include anthracycline, alkylating agents, an anti-microtubule agent taxane, and an anti-metabolite fluorouracil (5-FU), are the mainstay of systemic treatment for TNBC.[9, 10] However, chemotherapies are cytotoxic to healthy tissues and resistance occurs eventually in a significant portion of patients and lead to relapse of them. It is urgent to explore targeted therapeutic strategies for TNBC due to its poor prognosis and rare effective therapies [9, 11, 12]. Targeted therapy is a promising pursuit to reduce toxicity in patients by delivering drugs directly to tumor cells and overcome

drug resistance by increasing retention inside cells. Recently, a few newly targeted therapies for TNBC have been approved, including the poly (ADP-ribose) polymerase (PARP) inhibitors olaparib and talazoparib for germline BRCA mutation associated breast cancer (gBRCAm-BC)[13-18] and immune checkpoint inhibitors atezolizumab (anti-programmed death ligand-1; PDL1) and pembrolizumab (anti-programmed cell death-1; PD1) in combination with chemotherapy drugs.[13-16] These targeted therapies improve overall survival of TNBC patients carrying a BRCA mutation or PDL1 by 2-8 months,[17-19] whereas have shown incidence of adverse events,[20] can be resistant by tumor cells, and only benefit 35% of TNBC patients.[13-16, 19] Hence, it is necessary to utilize other targets in TNBC to develop a novel targeted drug delivery system.

Urokinase-type plasminogen activator receptor (uPAR), also known as CD87, is encoded by the PLAUR gene.[21] uPAR was first identified as the cell surface receptor for urokinase plasminogen activator (uPA) ligand,[22, 23] and mainly be responsible for degradation of extracellular matrix (ECM) components by uPA proteolytic activity.[24] uPAR is involved in ECM degradation, invasion and metastasis of malignant tumors, tumor angiogenesis and cell proliferation.[25-28] High uPAR expression has been shown in most solid tumor tissues, such as breast, lung, liver and pancreatic tumors.[29-31] High levels of uPAR have been linked to worse prognosis of breast cancer patients.[29] MDA-MB-231 cell line, which was derived from invasive human TNBC tumors, showed higher uPAR expression compared to other types of breast cancer cells.[29] Whereas MDA-MB-453, which was derived from less aggressive breast tumors, showed low uPAR expression.[32] Moreover, uPAR is overexpressed in cancer-associated stromal cells such as fibroblasts, macrophages, and endothelial cells.[33-35] Therefore, this makes uPAR a

potential target for targeted drug delivery system to kill both cancer cells and cancer-associated stromal cells.

Cationic polyamidoamine (PAMAM) dendrimers were widely used as nonviral gene carriers.[36-39] This nanostructure has been reported has high drug delivery efficacy and is available for drugs, gene, and protein therapeutics and can carry multiple payloads including imaging agent to endow multifunction.[40-42] In addition, it has been shown that hyperbranched generation 2 (G2) PAMAM dendrimer crosslinked via an amine-reactive, cleavable, homobifunctional linker DSP (3,3′-Dithiodipropionic acid di(N-hydroxysuccinimide ester)[43] and polyethylene glycol (PEG)[44, 45] (i.e., G2-DSP-PEG, or simply GDP) has a similar payload to generation 5 (G5) but has lower cytotoxicity.[46]After endocytosed through cell membrane, DSP of GDP can be readily GSH-triggered cleaved in cytoplasm, making it degradable.[46] GDP will have better capacity for drug or gene delivery as high generation PAMAM dendrimers, but lower cytotoxicity and GSH-triggered release profile.[36, 46] Collectively, we can utilize GDP as a powerful vehicle to conjugate with uPA binding domain and deliver anticancer gene or drug into tumor to yield an effective anticancer drug delivery system that has the potential to be applied for treating TNBC.

GTI-2040 (simply referred to as GTI) is a 20-mer phosphorothioate antisense oligonucleotide (5'-GGCTAAATCGCTCCACCAAG-3')[47] that is complementary to coding region in the mRNA of ribonucleotide reductase β2 subunit (R2) to induce RNase H cleavage.[48-50] Ribonucleotide reductase enzymes (R1 and R2)[51, 52] are responsible for the reduction of ribonucleotides to deoxyribonucleotides which is involved in DNA replication and repair.[53, 54] Increased R2 activity is highly associated with tumor cell

growth and malignant transformation in breast cancers including TNBC and has emerged as a key target for anticancer therapy.[55-60] R2 inactivation has been used as monotherapy or a combination with chemotherapies for various cancers in clinical trials.[56, 61-63] Recently, several R2 inhibitors including GTI through mRNA knockdown have entered clinical trials for cancer treatment.[61, 64-68] It has been demonstrated that GTI can decrease mRNA and protein levels of R2 and inhibit tumor growth in vitro and in vivo.[48] Phosphorothioate modification throughout the entire GTI expands the effective molecular lifetime by minimizing intracellular nuclease degradation for over 24 hours.[49, 69, 70] Furthermore, GTI combined with other chemotherapies has been investigated in phase I and phase II clinical trials for the promising treatment of cancers.[71-78] However, antisense oligonucleotide has low membrane permeability, and lacks an effective delivery system to against cancer in clinics.[71-78] GTI is an ideal model drug to test whether our uPA-mediated drug delivery system can improve GTI delivery and killing efficiency in TNBC.

Collectively, in this study, we synthesize uPA-mediated drug delivery system by conjugating cross-linked G2 dendrimers and uPA binding domain to carry GTI antisense oligonucleotide (GDP-uPA/GTI, Figure 1). Characterization and tumor-targeted capacity of this system are tested and assessed in vitro and in vivo model. Overall, this uPA-mediated drug delivery system may be a better vehicle for GTI to target TNBC cancer cells and cancer-associated stromal cells and a potential way to improve the therapeutic efficiency in the clinic and eliminate side effects.

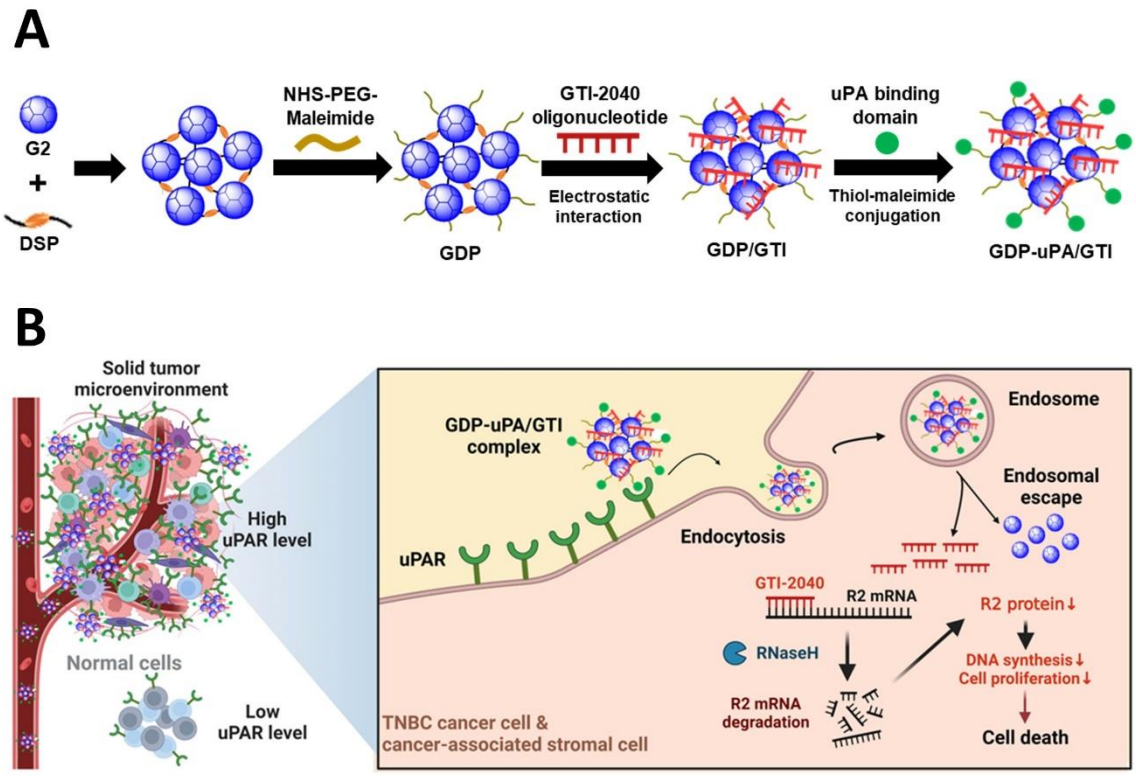

Figure 1. Schematic illustration of uPA-mediated targeted gene delivery system preparation route and its proposed strategy on treating TNBC. (A) Synthesis process of GDP-uPA/GTI complex. (B) GDP-uPA/GTI nanostructure is proposed to distribute to uPAR highly expressed tumor site through blood stream. After being uptake by TNBC cells and cancer-associated stromal cells via endocytosis, GTI can be released from GDP-uPA/GTI complex and knockdown human R2 mRNA in cytoplasm, which leads to reduced level of R2 protein and further results in cell death. G2: polyamidoamine generation 2 dendrimers; DSP: disulfide containing linker; GDP: G2-DSP-PEG; GDP/GTI: GDP carrying GTI; GDP-uPA/GTI: GDP-uPA carrying GTI. R2: ribonucleotide reductase β2 subunit.

2. MATERIALS AND METHODS

2.1. MATERIALS

Disulfide containing linker (3,3' -dithiodipropionic acid-di(N-succinimidyl ester), DSP) was synthesized in our lab. Polyamidoamine generation 2 dendrimer (PAMAM G2) was purchased from Nanosynthons (Mt Pleasant, MI, USA). NHS-PEG [MW=3400

$gmol^{-1}$] and NHS-PEG-Maleimide [MW=3497 $gmol^{-1}$] were purchased from RuixiBiotechCo.Ltd (Xi' An City, Shaanxi, China). uPA binding domain (DCLNGGTCVSNKYFSNIHWCN, 21 amino acids) was synthesized by LifeTein (Somerset, NJ, USA). GTI (5'- G*G*C*T*A*A*A*T*C*G*C*T*C*C*A*C*C*A*A*G -3', 20 nucleotides, * = phosphorothioated backbone link) and 3'-end Cy5 modified GTI were synthesized by Alpha AND (Montreal, Quebec, Canada).

2.2. CELL LINES & CELL CULTURE

MDA-MB-231 (#HTB-26, a TNBC cell line), MDA-MB-453 (#HTB-131, a non-TNBC breast cancer cell line), and HCC2218 (#CRL-2343, a mammary gland carcinoma fibroblast cell line) cell lines were purchased from American Type Culture Collection (ATCC, Manassas, VA, USA). Cell lines were maintained with RPMI-1640 medium (from ATCC) supplemented with 10% fetal calf serum (FCS) and 1% Penicillin/Streptomycin (P/S) at 37°C and 5% CO2.The cell culture reagents described above were purchased from Cytiva (Marlborough, MA, USA). Cells were passaged every three to five days in flasks.

2.3. ANIMALS

5-week-old female athymic nude mice (J:Nu) were purchased from Jackson Laboratory (Bar Harbor, ME, USA) and maintained at the S&T vivarium (Rolla, MO, USA). The mice were maintained in microisolated cages on ventilated racks in 12 hours light/dark cycle in a temperature-controlled room (18 – 22 ˚C) and given free access to food and water. All maintenance and experiment procedures followed the instructions

and regulations in an IACUC protocol approved by Institutional Animal Care and Use Committee of Missouri University of Science and Technology (IACUC reference No.: 197-22).

2.4. SYNTHESIS AND FUNCTIONALIZATION OF DENDRIMERS

Four types of nanostructure were synthesized: cross-linked PAMAM G2 (G2-DSP-PEG; or simply GDP), uPA-functionalized cross-linked PAMAM G2 (G2-DSP-PEG-uPA; or simply GDP-uPA), GDP carrying GTI (GDP/GTI), and GDP-uPA carrying GTI (GDP-uPA/GTI).

The final compound, GDP-uPA/GTI, was synthesized following the synthetic route described in Figure 1A. Firstly, disulfide containing linker (DSP) was dissolved in dimethyl sulfoxide (DMSO) and dropwise added into the PAMAM G2-containing PBS solution to make a molecular ratio 1:1 mixture.[46] The mixture was stirred at room temperature overnight. An appropriate amount of NHS-PEG-Maleimide [MW=3497 $gmol^{-1}$] was added into the mixture to make the molar ratio of PEG and NH_3 become 15:128 and stirred overnight.[79] The mixture was then dialyzed against DI water using 3.5 kDa dialysis tubing (Repligen, Boston, MA, USA). Outside DI water was changed every 6~12 hr, for three times. After freeze-dried at -20°C overnight, the GDP was obtained as a white powder, which was stored in -20°C for further use. Appropriate amount of GDP powder was dissolved in DI water and mixed with GTI solution in DI water to make the weight ratio of GDP and GTI become 5:1 and incubated for 30 min for electrostatic interaction to form GDP/GTI complex. GDP/GTI was then mixed with uPA solution in DI water to make the molar ratio of PEG-Maleimide and uPA become 1:1 and incubated

for 15 min for conjugation through thiol-maleimide click reaction to form GDP-uPA/GTI.

Following similar procedures, nanostructure without uPA functionalization and/or GTI (GDP, GDP/GTI or GDP-uPA) were synthesized for use as control.

2.5. CHARACTERIZATION OF FUNCTIONALIZED DENDRIMERS

Synthesized GDP in D_2O were analyzed with proton nuclear magnetic resonance (1H NMR; As-cend™400, from Bruker, Billerica, MA, USA). The biocompatibility of GDP in TNBC cells was assessed with MTT assay as shown in the below section. Transmission Electron Microscope (TEM; JEOL JEM-1400, at University of Missouri, Columbia) was performed to assess morphology and size distribution of the final compound GDP-uPA/GTI in DI water. Size distribution of GDP-uPA/GTI in TEM images taken from six different imaging fields (with total n=725 nanoparticles) was then measured by ImageJ software and presented in a histogram by SigmaPlot software.

2.6. GEL RETARDATION ANALYSIS

GDP (0.25~20 μg) and GTI (1 μg) were mixed at various weight ratios from 0.25:1 to 20:1 at pH 7.4 in PBS buffer and incubated at room temperature for 30 min. The GDP/GTI complex was mixed with 6X loading buffer and then analyzed using electrophoresis assay on 1.2% aga-rose gel that contained ethidium bromide (EtBr) in TBE buffer. The electrophoresis was performed at a voltage of 100V for 10 min. The GTI bands were detected by ChemiDoc XRS+ System (Bio-Rad, Hercules, CA, USA). Naked GTI was used as a control.

2.7. STABILITY OF GDP/GTI COMPLEX AGAINST DNASE I

The naked GTI and GDP/GTI complex were both incubated with DNase I (0.25 µg/mL) for 10, 30, or 60 min at room temperature. Each sample was mixed with 6X loading buffer and then analyzed using electrophoresis assay on 1.2% agarose gel that contained ethidium bromide (EtBr) in TBE buffer. The electrophoresis was performed at a voltage of 100V for 10 min. The GTI bands were detected using ChemiDoc XRS+ System.

2.8. HEPARIN-COUPLED ETHIDIUM BROMIDE FLUORESCENT ASSAY

The release of GTI from GDP/GTI at neutral (7.4) and acidic (5.6 and 6.8) pH conditions were assessed using heparin-coupled EtBr fluorescent assay. In a black 96 well plate, GTI (1 µg/well) and EtBr (1 µg/well) were mixed in PBS buffer to achieve a total volume of 30 µL/well. The plate was incubated at room temperature for 15 min. GDP (5 µg/well) was then added into each well to achieve a total volume of 60 µL/well and incubated for 15 min. The 40 µL heparin solution with different concentrations (0, 2, 4, 8, 10, 20, 30, 40, or 50 U/mL) was added to GDP/GTI to achieve the final volume of 100 µL/well. Finally, the plate was incubated for 30 min. The fluorescence intensity of EtBr (Ex=360 nm/Em=590 nm) was determined with a microplate reader (FLUOstar Omega, from BMG Labtech, Cary, NC, USA). The fluorescence values were normalized to GDP/GTI without heparin group.

2.9. CELLULAR UPTAKE STUDIES

To study cellular uptake mechanism of GDP/GTI, pharmacological inhibitors of endocytic pathways[80] were used. MDA-MB-231 cells ($8x10^4$ cells/well) were seeded in a 24-well plate and incubated overnight. Cells were treated with either one inhibitor: chlorpromazine (clathrin-mediated endocytosis inhibitor),[81, 82] nystatin (caveolae-mediated endocytosis inhibitor),[83] or EIPA (5-[N-ethyl-N-isopropyl] amiloride; macropinocytosis inhibitor)[84, 85] in completed medium at 37°C for 1 hr and washed with PBS for three times. Cells were then treated with GDP/GTI (25 µg/mL FITC-labeled GDP with 5 µg/mL GTI) at 37°C for another 1 hr. Cells were collected and washed with PBS for three times before analyzed by CytoFLEX Flow Cytometer (Beckman Coulter, Indianapolis, IN, USA). To test cellular uptake of GDP and GDP-uPA by different cell lines, MDA-MB-231, MDA-MB-453, and HCC2218 cells ($2x10^5$ cells/well) were seeded in a 6-well plate and incubated overnight. Cells were treated with GDP or GDP-uPA (both labeled with FITC) for 24 hr, and then collected and washed with PBS for three times before analyzed by CytoFLEX Flow Cytometer.

For cellular uptake of dendrimers and GTI, MDA-MB-231 cells ($2x10^5$ cells/well) were seeded in a 6-well plate and incubated overnight. Cells were treated with PBS, GTI only, GDP, GDP/GTI, or GDP-uPA/GTI (dendrimer was labeled with FITC; GTI was labeled with Cy5) for 6 hr, and then collected and washed with PBS for three times before analyzed by CytoFLEX Flow Cytometer.

Intracellular trafficking and visualization of cellular uptake were performed using confocal microscopy (A1R HD/Ti2E, from Nikon Instruments Inc., Melville, NY, USA). For intracellular trafficking, MDA-MB-231 cells ($3x10^4$ cells/well) were seeded in an 8-

well chambered cover-glass system and incubated overnight. After the incubation GDP/GTI (25 µg/mL GDP with 5 µg/mL Cy5-labeled GTI) for 2 or 6 hr, cells were stained with a mixture of Hoechst3342 (1 µg/mL) and LysoTracker™ Deep Red (50 nM, from Invitrogen) at 37°C for 30 min and washed with PBS for three times before imaging by confocal microscopy.

For visualization of cellular uptake by different cell lines, MDA-MB-231, MDA-MB-453, or HCC2218 cells ($3x10^4$ cells/well) were seeded in an 8-well chambered cover-glass system and incubated overnight. After the incubation with FITC-labeled GDP/uPA (25 µg/mL) for 1, 6, or 24 hr, cells were stained with Hoechst3342 (1 µg/mL) at 37°C for 30 min and washed with PBS for three times before imaging.

For visualization of GTI cellular uptake, MDA-MB-231 cells ($3x10^4$ cells/well) were seeded in an 8-well chambered cover-glass system and incubated overnight. After the incubation with PBS, GTI only, GDP/GTI, or GDP-uPA/GTI (25 µg/mL dendrimers; 5 µg/mL Cy5-labeled GTI) for 24 hr, cells were stained with a Hoechst3342 (1 µg/mL) at 37°C for 30 min and washed with PBS for three times before imaging. NIS-Elements AR Software (Nikon) was used for image analysis.

2.10. WESTERN BLOT

Cells were harvested and lysed with RIPA supplemented with protease inhibitor cocktail (1:100) and phosphatase (1:100). Following incubation for 30 min at 4°C, cell lysates were centrifuged for 15 min at 11,000 g (Micromax RF Centrifuge, from Thermo Fisher Scientific, Waltham, MA, USA) at 4°C. The concentrations of protein were measured using the BCA assay. Equal amounts of protein (20 µg protein with 2x loading

dye/well) were electrophoretically separated by SDS–PAGE (12%) and transferred to PVDF membranes by Power Blotter XL System (Invitrogen, Waltham, MA, USA). Membranes were then blocked with 5% skimmed milk in Tris-buffered saline with 0.1% Tween-20 (TBST) for 2 hr at room temperature. After washing with TBST three times for 5 min, membranes were incubated with primary antibodies (anti-human uPAR, from Invitrogen; anti-human beta-actin, from Cell Signaling, Danvers, MA, USA) overnight at 4°C, followed by a 1-hr incubation with HRP-conjugated secondary antibodies. ECL substrate was added on the PVDF membrane before analyzed by ChemiDoc XRS+ System.

2.11. MTT ASSAY

Biocompatibility of GDP and killing efficiency of GTI complex were determined using thiazolyl blue tetrazolium bromide (MTT assay, purchased from Bio-Techne, Minneapolis, MN, USA). For biocompatibility test, MDA-MB-231 cells were seeded at $1x10^4$ cells/well in a 96-well plate and incubated overnight. Cells were then treated with various concentrations (0-400 µg/mL) of GDP for 24 hr. For killing efficiency test, MDA-MB-231 cells were seeded at $1x10^4$ cells/well in a 96-well plate and incubated overnight. Cells were then treated with PBS, GTI only, GDP/GTI, or GDP-uPA/GTI group for 6 hr. After the treatment, 20 µL of MTT solution (to final concentration 0.5 mg/mL) was added to each well of 96-well plate and incubated at 37°C for 2 hr. To solubilize the purple formazan crystals, 200 µL of DMSO was added to each well after removing the medium and MTT solution. The optical density (OD) of each sample at 570

nm was measured using a microplate reader. Cell viability was normalized with PBS treated group.

2.12. REVERSE TRANSCRIPTION-QUANTITATIVE POLYMERASE CHAIN REACTION (RT-QPCR)

Total RNA extraction of cells was performed with TRIzol™ Plus RNA Purification Kit (Invitrogen) with DNase I treatment at room temperature for 15 min and stored in nuclease-free water at -80°C. The quality and concentration of RNA were determined using a microvolume spectrophotometer (NanoDrop™ OneC, from Thermo Fisher Scientific). RT-qPCR of template RNA was performed with TaqMan™ RNA-to-CT™ 1-Step Kit (Applied Biosystems, Foster City, CA, USA). Each reaction was prepared on a total volume of 10 µL, including RNA template (40 ng), TaqMan RT-PCR Mix (2X), TaqMan Gene Expression Assay (20X; beta-actin, #Hs99999903_m1; human R2, #Hs00357247_g1), TaqMan RT Enzyme Mix (40X), and nuclease-free H_2O. The mixtures were heated at 48°C for 15 min and 95°C for 10 min, followed by 40 cycles (95°C for 15 sec, 60°C for 1 min) using a QuantStudio 3 Real-Time PCR System (Applied Biosystems). Data was analyzed with QuantStudio™ Design and Analysis Software (Applied Biosystems). Gene expression of human beta-actin was used for normalization.

2.13. ESTABLISHMENT OF TNBC ORTHOTOPIC XENOGRAFT MICE MODEL

6-week-old female nude mice were weighed and then anesthetized with isoflurane. When adequate anesthesia had been achieved, MDA-MB-231 cells (5×10^6

cells/200 µL in 10% Matrigel; Corning, NY, USA) were injected into the 4th right mammary fat pad in each mouse with an insulin syringe with fixed needle (31G x 5/16'', from Medline, Northfield, IL, USA) for generating mammary gland tumor [86]. Tumor diameters were serially recorded with a digital caliper every 2 days, and tumor volumes were calculated with the formula: tumor volume (mm^3) = 0.5×length (mm) × width × width (mm^2). Body weights were recorded every 2 days. These mice develop orthotopic tumors to 40 mm^3 in around 4 weeks.

2.14. BIODISTRIBUTION STUDY

After the tumor grew to 40 mm^3, mice were then randomized into groups and received different treatments (PBS or GDP-uPA) by intravenous (IV) injection into the lateral tail vein. GDP-uPA (200 µg/20 g mice) was labelled with IRDye800cw (weight ratio 10:1; Ex:745/Em:810). Biodistribution of GDP-uPA was monitored at different time points (2, 6, 24, and 48 hr) after the IV injection using an AMI HTX imaging system (Spectral Instruments Imaging, Tucson, AZ, USA). Organs were collected after sacrifice of mice at 48 hr time point. The mice were anesthetized with isoflurane inhalation prior imaging.

2.15. THERAPEUTIC STUDY

When tumors grew to approximately 40 mm3, mice were randomized into groups and received different treatments (PBS or GDP-uPA/GTI) by IV injection into the lateral tail vein every day for two weeks (n=4~5). The dosage of GTI was 40 µg/20 g mice per day. Body weights were monitored every 2 days during the administration duration for

short-term safety evaluation. Tumor diameters were serially recorded with a digital caliper every 2 days, and tumor volumes were calculated as above. On the 15th day after injection, the mice were sacrificed, and xenograft tumors were dissected. The tumors were stained with hematoxylin-eosin (H&E) following standard protocols for histology analysis.

2.16. STATISTICAL ANALYSIS

All values are shown as mean ± standard deviation (SD). Comparisons between groups were evaluated using Student's t-test, and *: $p < 0.05$, **: $p < 0.01$, or ***: $p < 0.001$ was considered statistically significant.

3. RESULTS

3.1. CHARACTERIZATION OF FUNCTIONALIZED NANOSTRUCTURES

As shown in Figure 1A, multiple steps were involved in the synthetic route of GDP-uPA/GTI. G2 were crosslinked by the DSP to form a larger particle (G2-DSP). The bonds formed in this reaction can be readily cleaved in the cytoplasm, making it degradable.[87, 88] Subsequently, a heterobifunctional polyethylene glycol, NHS-PEG-Maleimide, was conjugated to the surface of the G2-DSP via NHS-amine chemistry[79] to form G2-DSP-PEG (GDP) nanostructure. GTI antisense oligonucleotide was added to be carried by GDP through electrostatic interaction (GDP/GTI). Finally, the targeted ligand uPA binding domain was introduced to the surface of the GDP/GTI by the click reaction between the thiol groups on the uPA and the terminal maleimide[89] to form GDP-

uPA/GTI complex. Following similar procedures, nanostructure without uPA functionalization and/or GTI (GDP, GDP/GTI, or GDP-uPA) was synthesized for use as a control.

The synthesized GDP was the basic material in this study and was characterized by ^{1}H NMR spectrum. As shown in Figure 2A, GDP had characteristic peaks for PAMAM G2 dendrimer (Ha−d for G2 scaffold methylene protons, Hb' and Hd' for G2 surface methylene protons adjacent to protonated NH_2 groups), DSP linker (He-f), and PEG (Hg). MTT result showed that GDP had a high biocompatibility (25 μg/ml) in MDA-MB-231 cells (Figure 2B), so 25 μg/ml concentration of dendrimers including GDP, GDP-uPA, GDP/GTI, GDP-uPA/GTI was used in all the following experiments. The morphology and size of our final compound GDP-uPA/GTI was assessed by TEM with 20000X and 120000X magnification (Figure 3A). The average diameter was measured to be approximately 16.45 nm (n=725, from six different imaging fields; Figure 3B), which was 5.6-fold larger than a single G2 particle. It suggests that the synthesized GDP-uPA/GTI had a completed nanostructure and united morphology and size.

3.2. GDP-uPA HAS A TARGETED CAPACITY TO uPAR HIGHLY EXPRESSED CELLS

To study the targeted capacity of GDP-uPA to uPAR highly expressed cells, cellular uptake of non-targeted dendrimer (GDP) or GDP-uPA in various cell lines that have different uPAR levels were tested. Expression of uPAR in different cell lines was quantified by western blot. Western blot results showed strongly high expression of uPAR in both MDA-MB-231 cells (TNBC cells) and HCC2218 cells (fibroblast cells) compared to MDA-MB-453 cells (non-TNBC cells) (Figure 4).

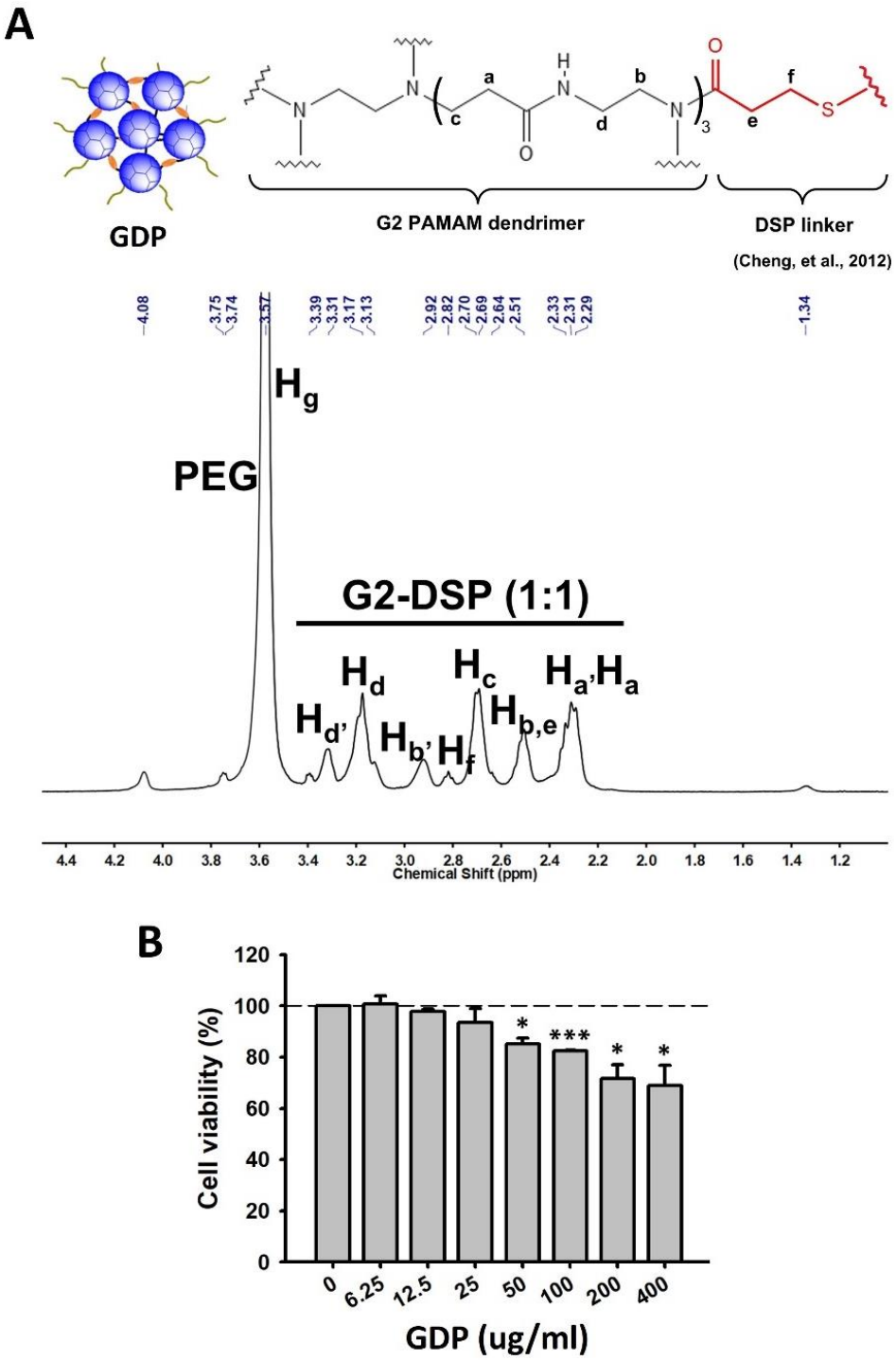

Figure 2. Characterization of the GDP. (A) 1H NMR spectrum analysis showed a uniform nanostructure of the GDP. (B) MTT assay showed the GDP had high biocompatibility (25 μg/ml) in MDA-MB-231 cells. All data are shown as mean ± SD (n=4). *: $p < 0.05$; ***: $p < 0.001$, compared with the control group.

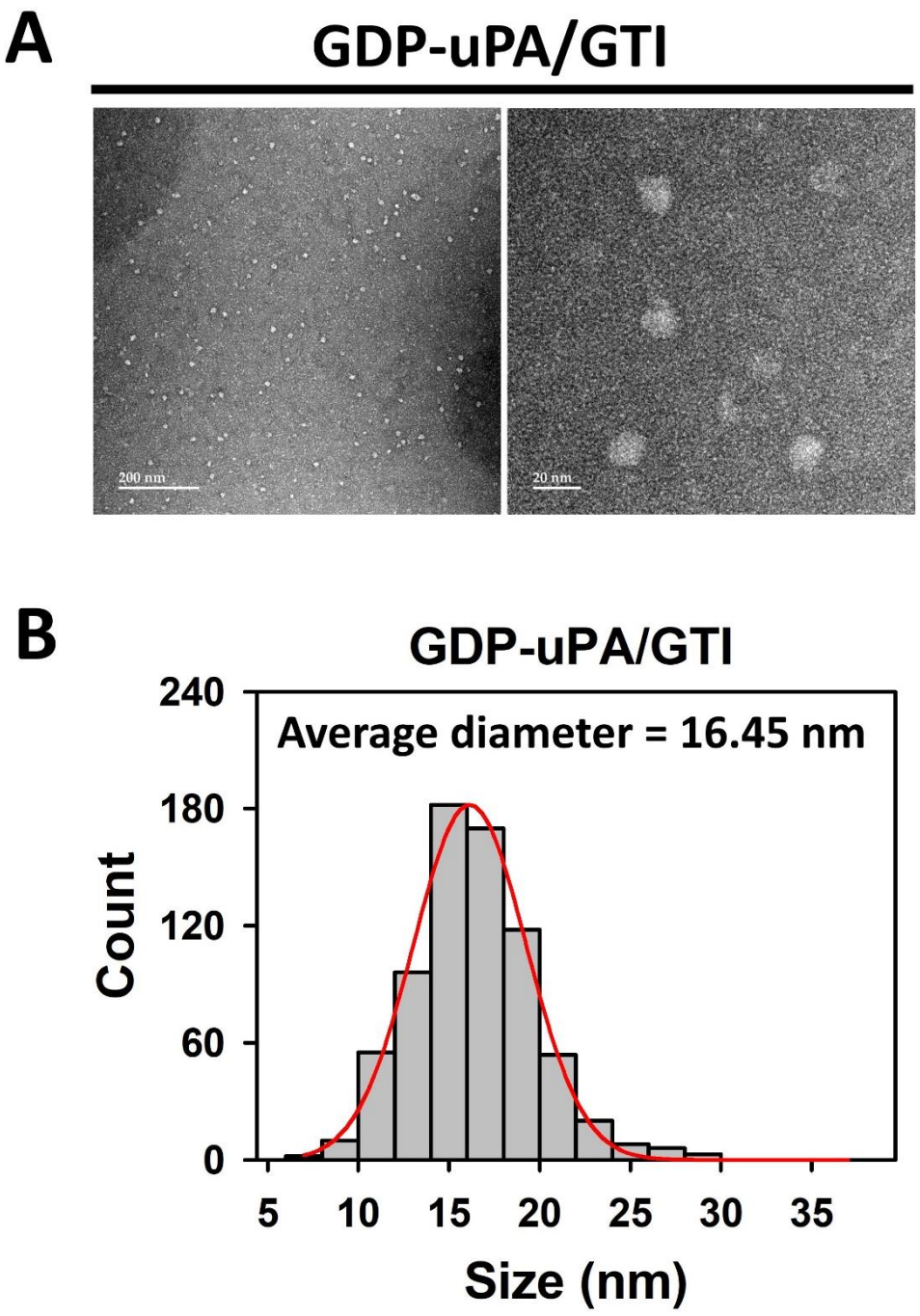

Figure 3. Morphology and size of the GDP-uPA/GTI. (A) TEM images and (B) the histogram of its size distribution showed the GDP-uPA/GTI had a uniform morphology and an average size of 16.45 nm diameter. magnification: 20000X (left) and 120000X (right). Scale bar: 200 nm (left) and 20 nm (right).

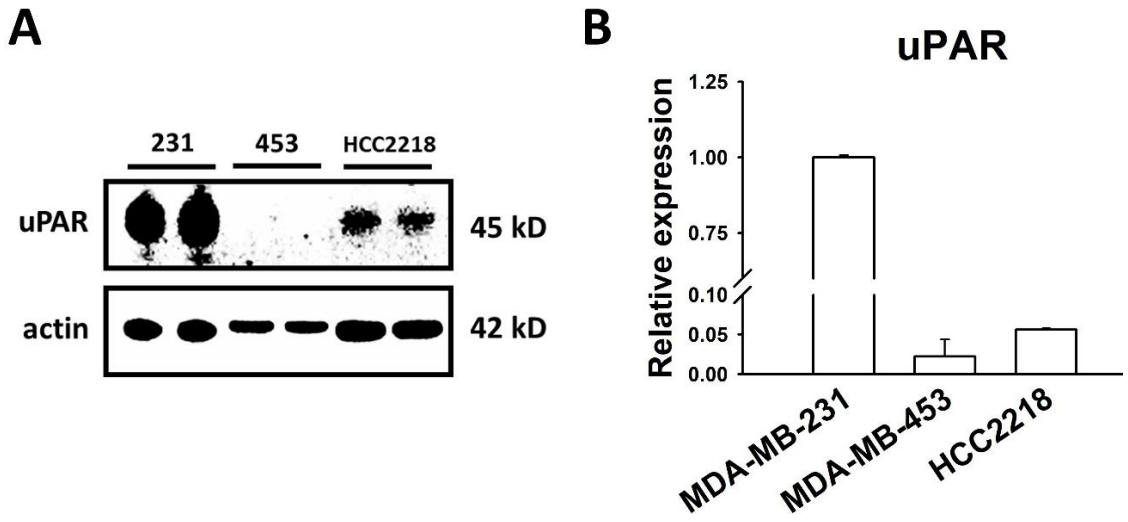

Figure 4. uPAR protein levels in different cell lines. (A) Western blot and (B) its quantification results showed that TNBC cells (MDA-MB-231) and fibroblast cells (HCC2218) highly expressed uPAR, whereas non-TNBC cells (MDA-MB-453) expressed low uPAR level. Actin was represented as a loading control. Quantification of uPAR was normalized with actin and then divided by the MDA-MB-231 group.

Images taken from confocal microscopy showed the faster and better uptake of GDP-uPA in MDA-MB-231 cells and HCC2218 cells than that in MDA-MB-453 cells (Figure 5A). In addition, flow cytometer analysis showed that GDP-uPA had a better uptake by MDA-MB-231 cells compared to non-targeted dendrimer (GDP) (Figure 5B). These results reveal that GDP-uPA has a targeted capacity and improved uptake efficiency in TNBC cells and fibroblast cells that highly express uPAR.

3.3. MECHANISMS OF UPTAKE AND RELEASE OF THE GDP/GTI COMPLEXES

To investigate the optimal mass ratio of GDP/GTI complex, the complexes were prepared at different mass ratios (0.25:1 to 20:1). Gel retardation results showed that dendrimers form stable complexes with GTI above the mass ratio of 5:1 (Figure 6A),

which was an appropriate ratio to be used in the following experiments. The electrophoresis results showed that GDP can protect GTI against DNase I (0.25 mg/ml) degradation (Figure 6B), which showed the potential to reduce the risk of the enzymatic degradation on GTI in future in vivo studies.

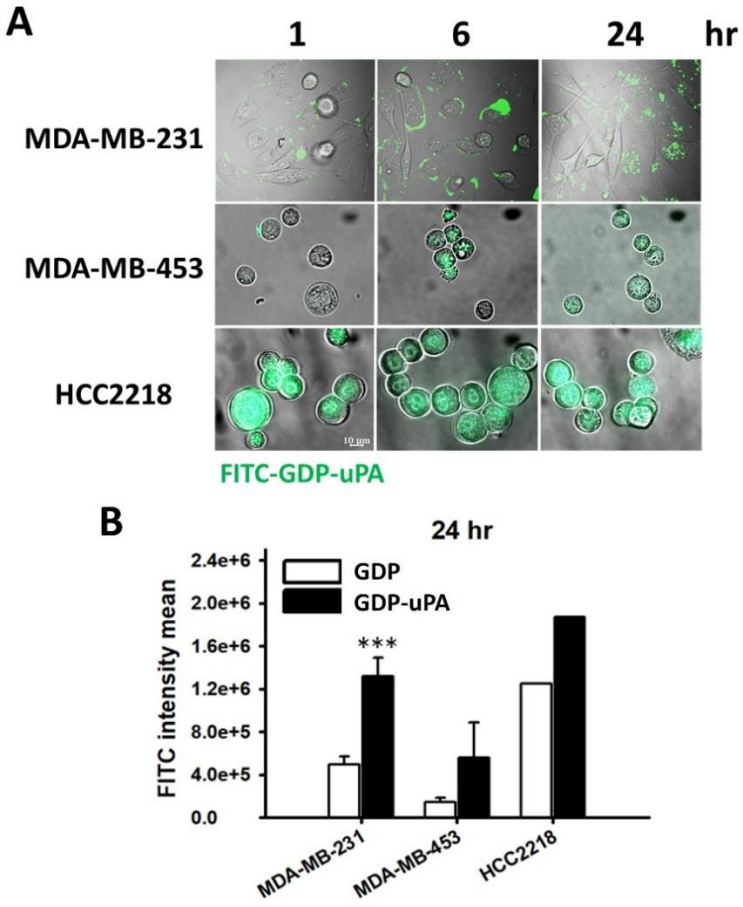

Figure 5. GDP-uPA has a targeted capacity to uPAR highly expressed cells. (A) Images taken by confocal microscopy and (B) flow cytometry results showed faster and better uptake of GDP-uPA in high-uPAR level cell lines including MDA-MB-231 and HCC2218. Also, GDP-uPA showed better uptake than non-targeted dendrimer (GDP) in MDA-MB-231 cells. Green: GDP-uPA; magnification: 60X; scale bar: 10 μm. All data are shown as mean ± SD (n=3). ***: $p < 0.001$, compared with the GDP group.

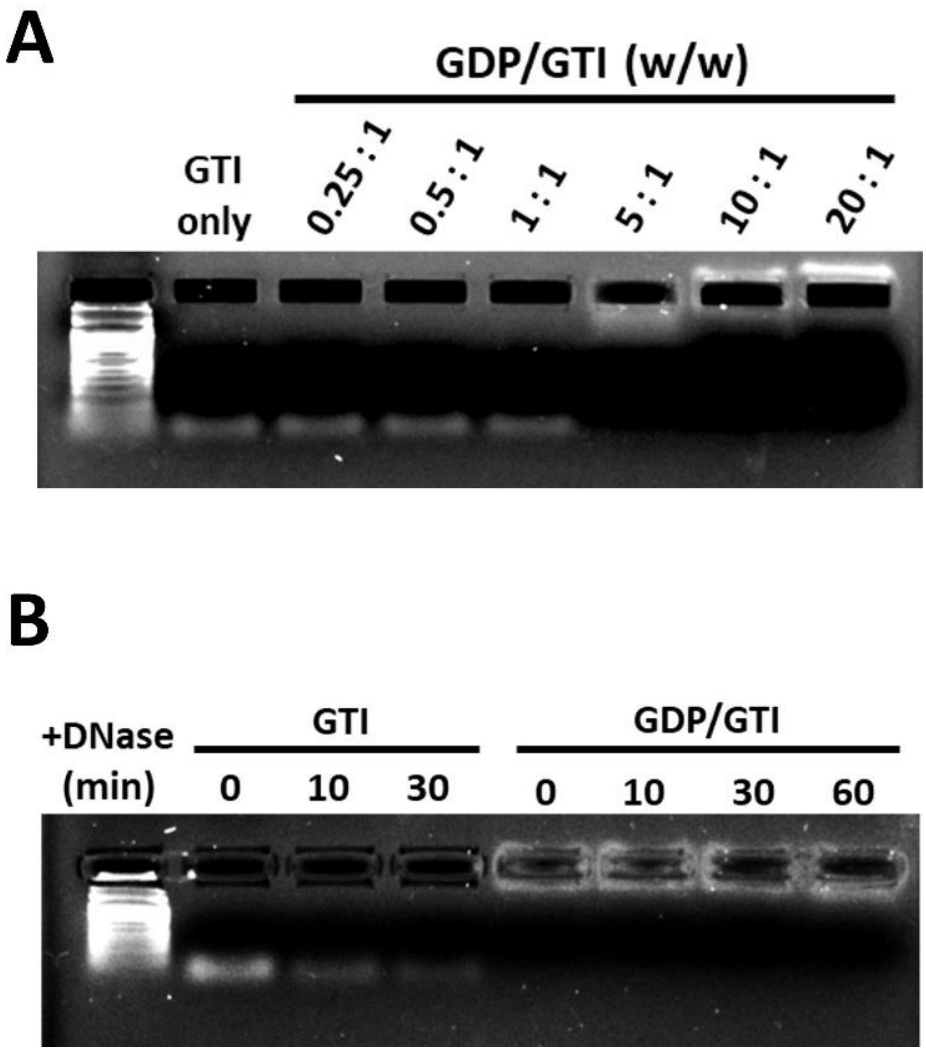

Figure 6. Optimal weight ratio of the GDP/GTI complexes. (A) Gel retardation results showed weight ratio 5:1 of GDP/GTI completely carry GTI. (B) GDP could protect GTI against DNase degradation. Lane 1: DNA ladder.

To study uptake and release mechanism of GDP/GTI complex, flow cytometer and EtBr fluorescent assay were performed, respectively. After chlorpromazine, nystatin, or EIPA was applied for 1 hr in priority to the GDP/GTI treatment, a significant reduction in the cell uptake of GDP/GTI complex was observed (Figure 7). The results suggest that clathrin-mediated endocytosis, caveolae-mediated endocytosis, and macropinocytosis are all actively involved in uptake of the GDP/GTI complex.

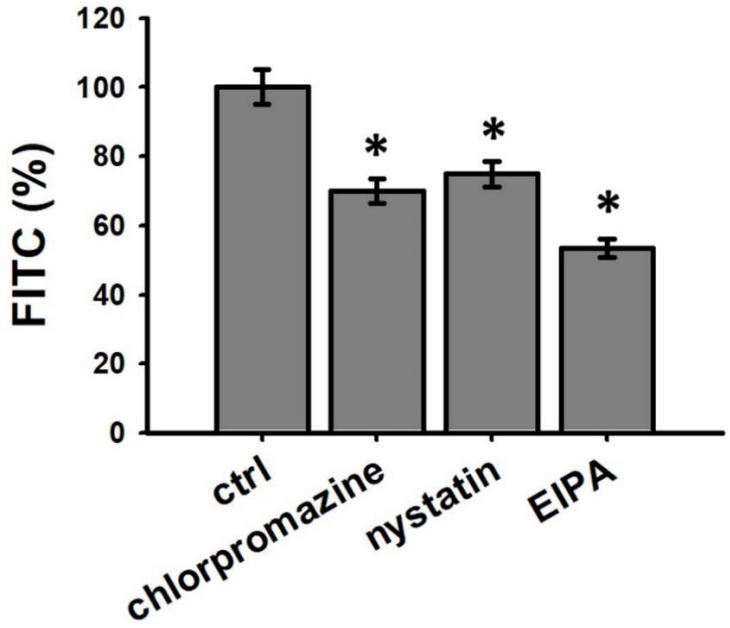

Figure 7. Internalization mechanisms of GDP/GTI in TNBC cells. Flow cytometry results showed that 1-hr pretreat of inhibitors of micropinocytosis, clathrin-mediated endocytosis, and caveolae-mediated endocytosis pathways significantly reduced the uptake of the GDP/GTI complex in MDA-MB-231 cells. It suggests micropinocytosis, clathrin-mediated endocytosis, and caveolae-mediated endocytosis pathways were all actively involved in the uptake of the GDP/GTI complex in MDA-MB-231 cells. Inhibitors: EIPA (macropinocytosis), chlorpromazine (clathrin-mediated endocytosis), and nystatin (caveolae-mediated endocytosis). All data are shown as mean ± SD (n=3~4). *: $p < 0.05$, compared with the control.

As shown in Figure 8, GDP/GTI complex forms easily and stably at neutral pH but disassembles readily under acidic conditions (pH 6.8 and 5.6). Also, the release potency of GTI from the complex was pH-dependent. It suggests that GDP/GTI may be stable in the blood, while being unstable and further disassemble in the acidic environment such as cancer microenvironment (pH 5.6~6.8),[90, 91] endosomes, and lysosomes, which enables dendrimer to release GTI when delivered into tumor site.

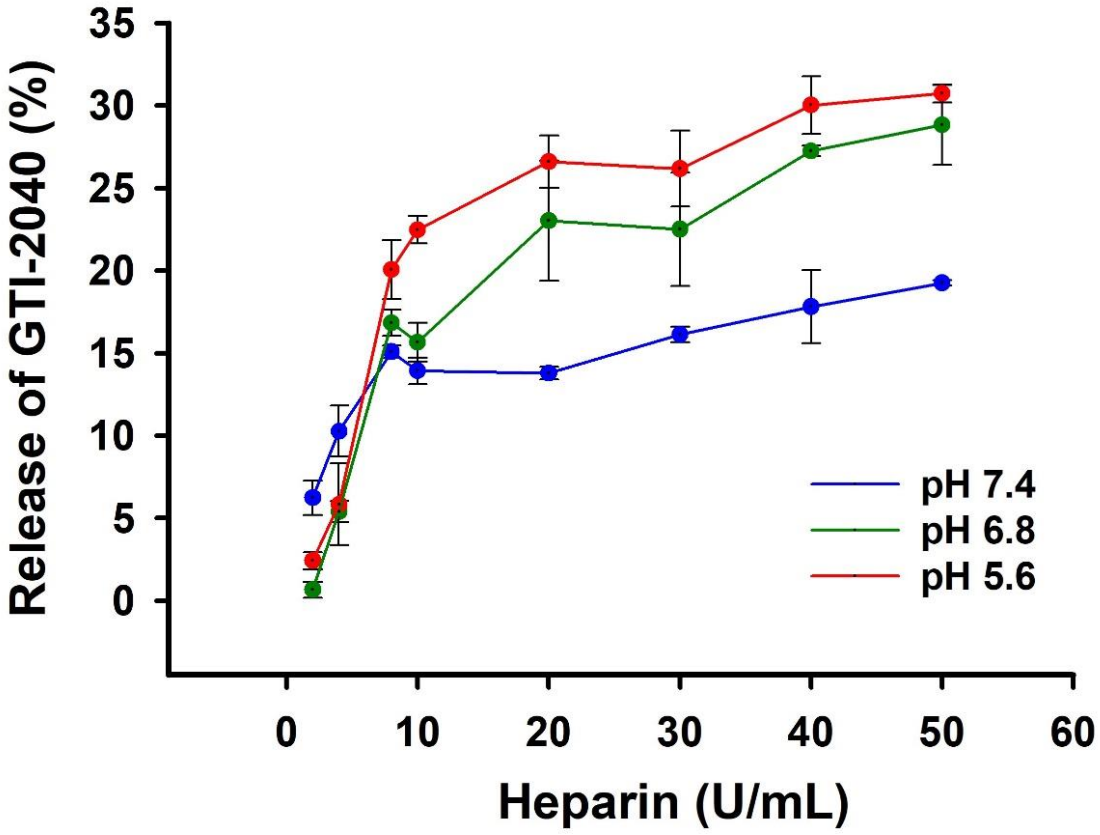

Figure 8. Release profile of GTI from GDP/GTI complex. Ethidium bromide fluorescent assay results showed that GDP/GTI complex was unstable in acidic environment (pH 5.6 and 6.8) and readily and easily disassembled compared to under the neutral condition (pH 7.4).

To study intracellular trafficking of GDP/GTI complex, the subcellular localization was assessed with confocal microscopy. Images taken by confocal microscopy showed the colocalization (yellow dots) of GDP/GTI complex (red) and Lysotracker (green) in MDA-MB-231 cells at the 2 hr time point, which reveals the trafficking of GDP/GTI complex into endosomes after 2 hr of treatment (Figure 9).

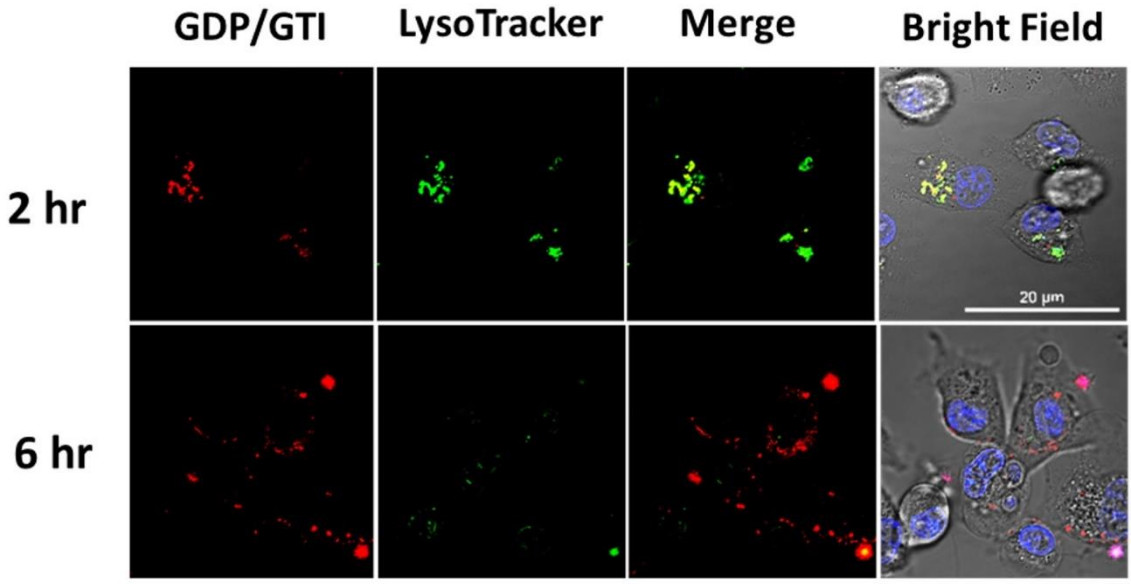

Figure 9. Subcellular localization of the GDP/GTI complex in TNBC cells. Images were taken by a confocal microscopy. The colocalization (yellow dots) of GDP/GTI and LysoTracker in MDA-MB-231 cells was observed after 2 hrs of treatment. After 6 hrs, GDP/GTI showed separation from the LysoTracker signals and remained in cytoplasm. Red: GTI; green: Lysotracker, representing lysosomes and endosomes; blue: nucleus; magnification: 60X; scale bar: 20 μm.

At the 6 hr time point, the red signal showed separation from the green signal of LysoTracker (Figure 9). Also, the reduced and shrinking green signals indicated a dissociation of endosomal caused by the proton sponge effect and led to endosomal escape.[92] The result represents the GDP/GTI getting into cells by endocytosis and the effective release of Cy5-labeled GTI from endosomes into cytoplasm. Release and separation of GDP/GTI from endosomes to cytoplasm are important for mRNA knockdown. It enables GTI to hybridize to the R2 mRNA in cytoplasm and further lead to R2 knockdown.[48]

3.4. GDP-uPA IMPROVES GTI DELIVERY AND KILLING EFFICIENCY ON TNBC CELLS

Flow cytometer results showed GDP-uPA/GTI had approximate 1.75 times better uptake of dendrimers by MDA-MB-231 cells than that of GTI only group and non-targeted GDP/GTI group (Figure 10A). Moreover, GDP-uPA/GTI improved the delivery efficiency of GTI up to 6-fold and 3-fold compared to the GTI only group and non-targeted GDP/GTI group, respectively (Figure 10B). The confocal microscopy images (Figure 10C) showed similar results that, after 6-hr treatment, GDP-uPA/GTI apparently enhanced delivery efficiency of GTI in MDA-MB-231 cells compared with the GTI only and GDP/GTI groups. Besides, a little more Cy5 signals could be observed in the GDP/GTI group compared to the GTI only group, which was consistent to the data from flow cytometry.

MTT results showed that GTI delivered by GDP or GDP-uPA significantly reduced cell viability of MDA-MB-231 cells by about 30% compared to the PBS group after 6-hr treatment, while the GTI only group had no difference with the PBS group (Figure 11). The results suggest that GDP-uPA can improve the killing efficacy of GTI in TNBC cells. The RT-qPCR results showed decreased human R2 protein expression on mRNA level by 95% in the GDP-uPA/GTI treated group compared to the PBS group, while other groups showed no significant differences (Figure 12). Collectively, it suggests that GTI delivered by GDP-uPA killed cells by 30% through knock-downing R2 mRNA expression.

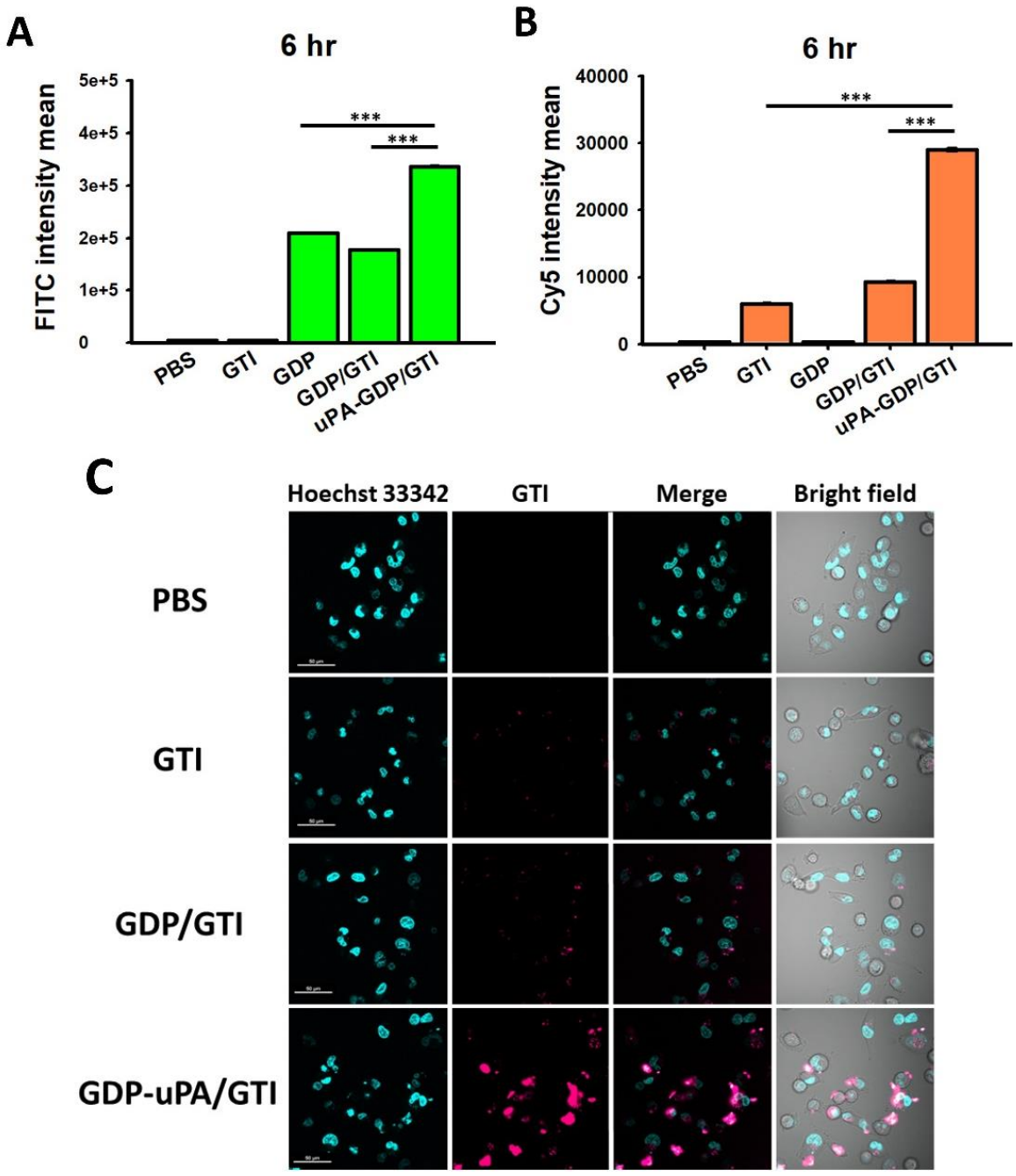

Figure 10. GDP-uPA/GTI improves GTI delivery in TNBC cells. Flow cytometry results showed (A) the GDP-uPA/GTI group had better uptake in TNBC cells and (B) further improved GTI delivery compared to the naked GTI and GDP/GTI groups. (C) Images taken by a confocal microscopy showed that GDP-uPA/GTI improved GTI delivery in TNBC cells compared to other groups. FITC: GDP or GDP-uPA; Cy5: GTI. Red: GTI; blue: nucleus; magnification: 60X; scale bar: 50 μm. All data are shown as mean ± SD (n=3~4); ***: $p < 0.001$.

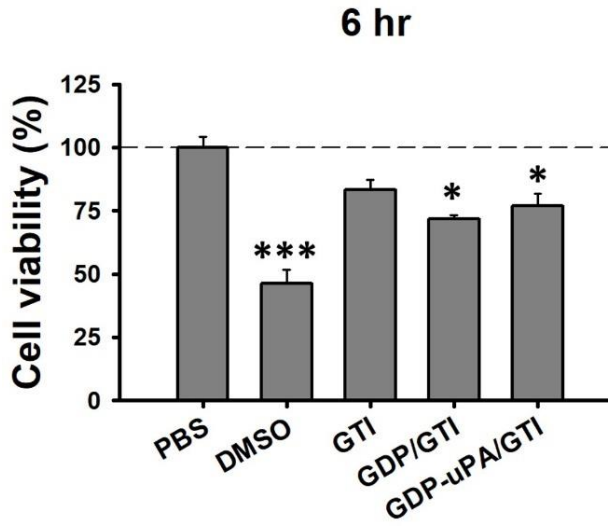

Figure 11. GDP-uPA/GTI improves killing efficiency on TNBC cells. MTT results showed that GTI delivered by dendrimers (GDP/GTI and GDP-uPA/GTI) significantly killed cells by ~30% after 6-hr treatment, whereas GTI only group did not. All data are shown as mean ± SD (n=3~4). *: $p < 0.05$; ***: $p < 0.001$, compared with the PBS.

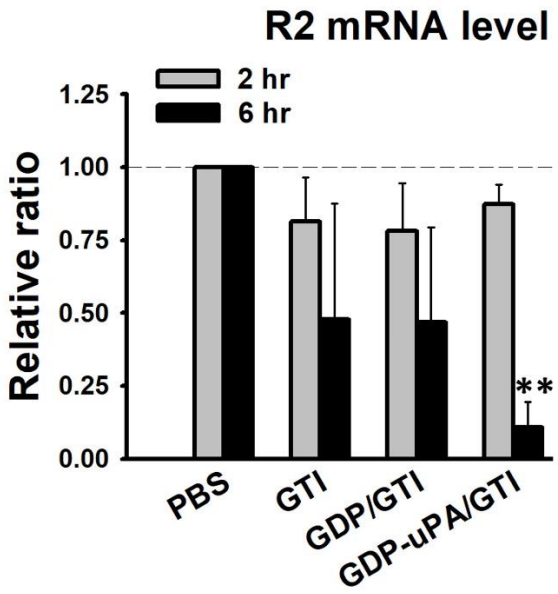

Figure 12. R2 knockdown by GDP-uPA/GTI in TNBC cells. GDP-uPA/GTI significantly knockdowned human ribonucleotide reductase component (R2) level in MDA-MB-231 cells after 6-hr treatment, while other groups did not. All data are shown as mean ± SD (n=3). **: $p < 0.01$, compared with the PBS.

3.5. GDP-UPA/GTI SHOWS TUMOR-TARGETED EFFICACY AND RESULTS IN TUMOR GROWTH INHIBITION IN THE TNBC XENOGRAFT MODEL

To investigate the tumor-targeted capacity and delivery efficiency of GDP-uPA, biodistribution of GDP-uPA was assessed in the TNBC orthotopic xenograft model generated from athymic nude mice. As shown in Figure 13A, IRDye-labeled GDP-uPA signals mainly distribute to the tumor site after 2 hr of IV injection at the tail and can accumulate at the tumor site for at least 48 hr. The other signals mainly distribute to the kidneys and liver (Figure 13B). Also, some signals are also observed in the lungs (Figure 13B), which may be due to the tumor metastasis occurring in the lungs that happens in TNBC model. These results suggest that GDP-uPA has tumor-targeted capacity and great retention in tumor and may be excreted by kidneys and liver in the future.

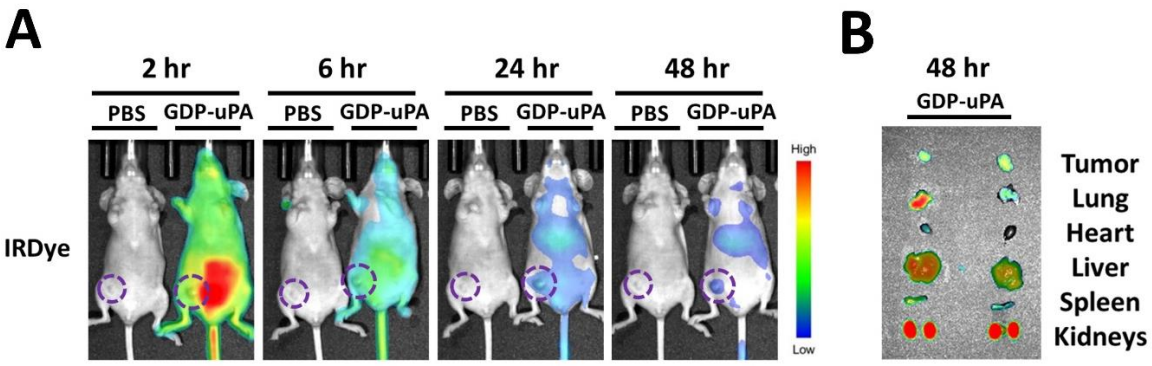

Figure 13. GDP-uPA/GTI shows tumor-targeted efficacy in the TNBC xenograft mice model. Biodistribution results including (A) whole body and (B) organs images taken by AMI HTX imaging system showed that GDP-uPA could be distributed by blood stream and targeted to tumor site in orthotopic TNBC xenograft mice model after 48 hr of IV. Injection. GDP-uPA signals were also observed in the liver and kidneys. Purple circle: tumor site. IRDye: GDP-uPA. Rainbow colors represent the live signal level.

For the therapeutic study of GDP-uPA/GTI, body weight and tumor size of TNBC xenograft mice model were monitored during the administration duration (Figure 14). There is no significant body weight drop during the GDP-uPA/GTI administration, which means the complex is safe for mice in a short-term study (Figure 14A). In addition, GDP-uPA/GTI significantly inhibits tumor growth during the administration compared to the PBS treated group (Figure 14B).

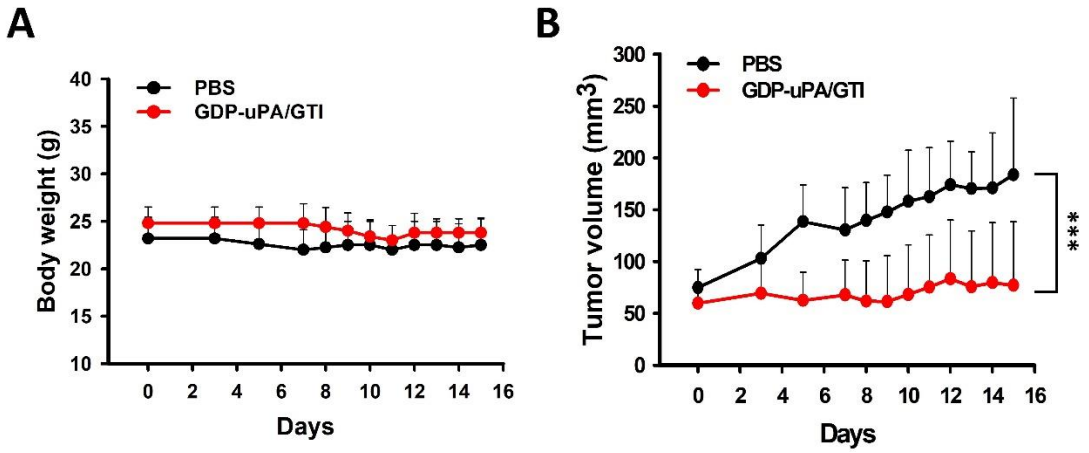

Figure 14. GDP-uPA/GTI results in tumor growth inhibition in the TNBC xenograft model. (A) There was no significant body weight drop during the GDP-uPA/GTI administration, which meant the complex was safe to mice in a short-term study. (B) GDP-uPA/GTI complex significantly inhibited tumor growth during the administration duration. Data are shown as mean ± SD (n=4~5). ***: $p < 0.001$, compared with the PBS group.

As shown in Figure 15, histology image of tumor in GDP-uPA/GTI treated group demonstrated much more apoptotic cells (arrow site: shrink nucleus surrounding by empty space) and incomplete tumor structure with fewer stromal cells (long shaped light pink cells), while the PBS group had solid structure and full of condensed stromal cells.

Collectively, it reveals that GDP-uPA/GTI can distribute and deliver GTI into tumor through blood circulation and inhibited tumor progression in the TNBC mice model.

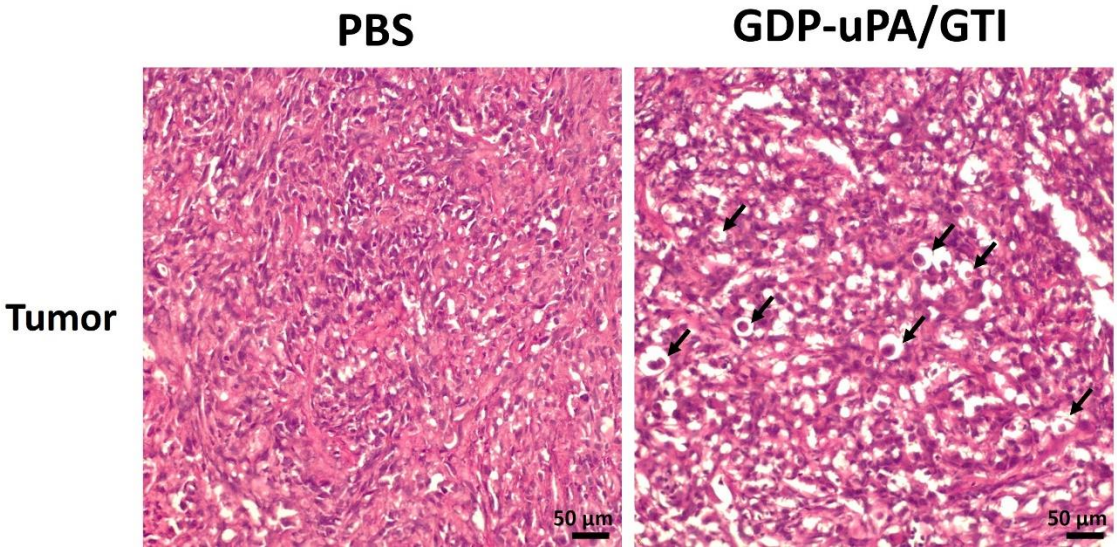

Figure 15. H&E histological images of tumor sections. The histological images showed that GDP-uPA/GTI group had more apoptotic cells and less stromal cells compared with the PBS group. Purple circle: tumor site. Scale bar: 50 μm. Magnification: 20X. Arrow: apoptotic cells.

4. DISCUSSIONS

In this study, we hypothesized that GDP-uPA nanostructure would have a targeted delivery capacity to uPAR highly expressed cells and tissues and would improve the delivery and killing efficiency of GTI in TNBC cells.

The western blot results showed that both MDA-MB-231 and HCC2218 cell lines expressed high uPAR level (Figure 4) and took more GDP-uPA compared to MDA-MB-453 cells did (Figure 5). However, MDA-MB-231 cells also demonstrated a higher uPAR level than HCC2218 cells did, whereas HCC2218 cells took more GDP-uPA than MDA-

MB-231 cells did (Figure 5). We speculate that it is because HCC2218 is a suspension cell line, while MDA-MB-231 is an adherent cell line. It is easier for nanoparticles to attach and be taken by HCC2218 cells, which have more available surface area and three dimensions morphology compared to adherent cells. Anyway, it does not change the fact that GDP-uPA has a targeted capacity and better uptake than non-targeted GDP nanostructure in TNBC cells. To overcome this kind of impediment in in vitro study to test targeted capacity, it is preferable to perform 3D culture spheroid model or organoid model that recapitulates many aspects of the complex structure and function of the corresponding in vivo tissue.[93] Still, *in vivo* study in an animal model for biodistribution is the best way to investigate the targeted capacity of drug delivery system.

The duration of treatment of cells with nanocomplexes and the time point at which samples are collected for analysis are important but are always difficult to determine. While GDP-uPA was taken up by TNBC cells and stromal cells after 1 h of treatment (Figure 5A), significant R2 mRNA knockdown by GDP-uPA/GTI occurred after 6 h of treatment (Figure 12).Thus, we analyzed samples by flow cytometry and cell viability assay at the 6-h post-treatment time point to obtain cell uptake and killing efficiency data. To obtain the most appropriate and consistent data, longer treatment durations (e.g., 12, 24, or 48 hours) could be conducted and studied in future studies to obtain more significant results.

To investigate the delivery improvement and killing efficiency of GDP-uPA/GTI in TNBC cells compared with the naked GTI and non-targeted GDP/GTI groups, cellular uptake studies and cell viability assay were performed. Our flow cytometry and confocal results showed that, after a 6-hr treatment, GDP-uPA/GTI group had significantly better

delivery of GTI (3-fold) in TNBC cells compared to naked GTI and non-targeted GDP/GTI groups did (Figure 10). Based upon these results, we initially anticipated that GDP-uPA/GTI group would lead to much more reduction in cell viability than GTI and GDP/GTI groups would do. However, the MTT results showed that both GDP/GTI and GDP-uPA/GTI could significantly reduce viability (by ~30%) of TNBC cells after 6-hr treatments, while the GTI only group could not (Figure 11). Taken together, this shows that the delivery efficiency of the GDP/GTI group may be sufficient for GTI to kill TNBC cells, although its delivery efficiency is only one-third that of the GDP-uPA/GTI group. Even so, GDP represents nonspecific delivery, whereas GDP-uPA has shown targeting ability to uPAR-high-expressing TNBC cells and stromal cells (Figures 4 and 5). Furthermore, the situation in the mouse model of TNBC will be different compared to the cell model, as it imposes more stringent conditions on the nanostructures in terms of blood circulation, tumor penetration, and retention.[94, 95] Therefore, in addition to cell models, it is necessary to examine the targeting ability and tumor inhibition efficiency of GDP/GTI and GDP-uPA/GTI nanocomplexes in TNBC mice models.

Our *in vivo* results demonstrated the biodistribution and a 48-hr retention of GDP-uPA nanostructure into the tumor site of a TNBC xenograft model (Figure 13). GDP-uPA/GTI showed a significant tumor growth inhibition (58.09% reduction compared to the PBS group) after the administration by IV injection for 14 days (Figure 14B). For further investigation of tumor-targeted and delivery efficacy between non-targeted GDP and GDP-uPA, more groups (PBS, GTI, GDP/GTI, GDP-uPA/GTI) were performed in the TNBC mice model (Figure A1 and A2). To be noted, this TNBC xenograft mice model was established by the same procedures written in the MATERIALS AND

METHODS section but using mice with older age (13-week-old) and they were IV injected with the nanostructures every two days, instead of every day, for two weeks, so this data was just a preliminary assessment of tumor-targeted and delivery efficacy using more treatment groups (n=5~6/group) and did not be included in the main content. As shown in Figure A1, only the GDP-uPA/GTI group, instead of the non-targeted GDP/GTI group, could distribute to the tumor site (purple circle in Figure A1A) and retain in the tumor for at least 48 hours. In addition, other signals could be observed mainly in the kidneys and liver at the 48 hr time point after the injection (Figure A1B), which suggested it might be excreted by kidneys and liver in the future. For the therapeutic study, body weight and tumor size of the TNBC xenograft mice model were monitored during the administration duration (Figure A2). There was no significant body weight drop during the administration of GTI, GDP/GTI, and GDP-uPA/GTI, which referred to the nanocomplexes were safe for mice in a short-term study (Figure A2A). As shown in Figure A2B and A2C, the GDP-uPA/GTI group significantly inhibited the tumor growth (51.89% reduction) during the administration compared to the PBS treated group, while no significant difference was observed among the PBS, GTI, and GDP/GTI groups. These preliminary studies showed that GDP-uPA nanostructure had a tumor-targeted capacity (Figure A1) and exhibited a better anti-tumor efficacy (Figure A2) when carrying GTI, whereas the non-targeted GDP nanostructure did not target the tumor and had less anti-tumor efficacy. It enables us to know the differences in tumor-targeted capacity and anti-tumor efficacy between the non-targeted GDP/GTI and GDP-uPA/GTI nanocomplexes.

To transform GDP-uPA/GTI into a clinically feasible treatment for TNBC, there is a critical need to determine the delivery mechanism of GDP-uPA into TNBC cells and the anti-tumor mechanism of GDP-uPA/GTI. Our future directions (Figure A3) are exploring the delivery mechanisms of GDP-uPA and the molecular mechanisms of R2 knockdown resulting from GDP-uPA/GTI, including the following five research aspects:

1) The intracellular degradation and dissociation of GDP. Disulfide cleavage of GDP is essential for the high releasing efficacy of GTI.[46] It has been known that glutathione (GSH) can cleave disulfide bonds, and GSH's intracellular concentration is 100-1000 times higher than extracellular.[87, 88, 96] It has been shown that GSH promoted GDP degradation by digesting crosslinkers among the nanostructure after getting into cytoplasm.[46] To verify whether the disulfide bonds of the GDP are degradable with GSH presence, DLS will be used to assess the size differences after incubation with different concentrations (1, 10, 100, 1000, and 10000 μM)[96] of GSH in DI water for 10, 30, or 60 min. The hydrodynamic size of degraded GDP is expected to decrease from 13.09 nm to 2.9 nm (single G2) after incubation with GSH.

2) To identify the interaction of GDP-uPA and uPAR on the cell membrane, competitive binding assay of GDP-uPA and uPA to uPAR will be adapted. MDA-MB-231 cells have been shown to express high uPAR levels and will be split into four groups (1×10^6 cells in 100 μL of staining buffer/group) in centrifuge tubes. His-tagged pro-uPA, GDP-uPA, and APC-conjugated anti-His antibody will be used for the aompetitive binding assay. Pro-uPA-bound cells will be detected using flow cytometry. We anticipate that a competitive binding assay will show the ability of GDP-uPA to inhibit APC-His-

tagged pro-uPA binding to uPAR, which reveals the interacting capacity of GDP-uPA to uPAR.

3) Our current data has shown some promising and supportive results of GDP-uPA and GDP-uPA/GTI compared to naked GTI and non-targeted GDP and GDP/GTI groups. However, it's necessary to include more control groups, such as scrambled GTI (sGTI) and Lipofectamine/sGTI (Lipo/sGTI) as negative controls, and Lipofectamine/GTI (Lipo/GTI) as a positive control to ensure a rigorous and reliable outcome. We will conduct the previous and future experiments (cellular uptake, R2 knockdown, and killing efficiency studies) with these control groups. We will obtain three scrambled sequences, including sGTI_1 (5'- ACGCACTCAGCTAGTGACAC -3'),[48] sGTI_2 (5'- ACGCCTCAATAGTACGAGCC- 3'), and sGTI_3 (5'- ACTGCCTAATCGAACGGCCA -3'), that are not complementary to human R2 mRNA but retain the same base composition ratio to GTI (5'- GGCTAAATCGCTCCACCAAG -3'). These sGTIs are generated randomly and have the weakest (or no) match with any mRNA in the mRNA pool for humans. To ensure the sGTIs do not affect R2 expression and cell viability in TNBC cells, the preliminary RT-qPCR and MTT assays will be conducted. One sGTI, two if available, will be chosen according to the results and used in the following experiments.

4) Molecular mechanism of R2 knockdown on killing TNBC cells will be determined (Figure A3). Based on the studies about R2 inactivation in other cancer models, R2 inactivation can lead to cell cycle arrest and apoptosis induction due to its inhibition in DNA synthesis.[62, 97-103] Flow cytometry analysis will be conducted using the Dead Cell Apoptosis Kit with Annexin V Alexa Fluor 488 & Propidium Iodide (PI) and

Cell Cycle Analysis Kit to study the molecular mechanism of R2 knockdown by GTI in TNBC cells.

5) Effects of R2 knockdown on proliferation- and apoptosis-related signaling pathways will be determined (Figure A3). R2 inactivation has been reported to downregulate MAPK and PI3K/AKT/mTOR signaling pathways related to cell proliferation,[97-99] and induce apoptosis involving pathways such as Bcl-2, BAX/BAK, and caspases pathways[100-103] in various cancer types including breast cancer, pancreatic cancer, lung cancer, cervical cancer, and leukemia. ELISA kits of MAPK, PI3K, AKT/p-AKT, mTOR/p-mTOR, Bcl-2, BAX/BAK, caspase-3/cleaved caspase-3, caspase-9/cleaved caspase-9 will be performed to study the effects of R2 knockdown by GTI on its downstream signaling pathways. Tumor samples from *in vivo* studies will also be processed and analyzed with these ELISA kits for signaling pathway studies.

The accomplishment of the future directions will give us a better understanding of molecular mechanisms results from R2 knockdown by GDP-uPA/GTI in anti-tumor effects *in vitro* and *in vivo*. In addition to the understanding of GDP-uPA/GTI delivery mechanisms, it will bring us more knowledge of possible combination therapies with R2 inhibitors, like GTI, to treat TNBC by combining R2 inhibitors with therapies that target signaling pathways that are complementary to those of R2 inactivation to achieve synthetic lethality in tumors. These outcomes can also be expanded into other types of cancer expressing high levels of R2.

5. CONCLUSIONS

In this study, uPA-mediated polyamidoamine dendrimer-based targeted drug delivery system was successfully synthesized and was easily prepared. GDP-uPA can be uptake faster and better by both TNBC cells and stromal cells that highly express uPAR, compared to lower uPAR expressing cells. In addition, GDP-uPA improved the transfection efficiency of anti-tumor nucleotic acids including GTI compared to non-targeted dendrimers (GDP) in TNBC cells and enhanced R2 knockdown efficiency. In an orthotopic TNBC xenograft mice model, GDP-uPA/GTI could be distributed by blood circulation and target to tumor site, and further significantly inhibited tumor growth during the administration duration.

Our study demonstrates that this GDP-uPA has great potential to become an efficient targeted delivery system and can be expanded and applied with different anti-tumor gene or drug to treat uPAR overexpressed cancers including TNBC.

REFERENCES

1. Siegel, R. L.; Miller, K. D.; Fuchs, H. E.; Jemal, A., Cancer statistics, 2022. *CA Cancer J Clin* **2022,** *72* (1), 7-33.

2. Siegel, R. L.; Miller, K. D.; Fuchs, H. E.; Jemal, A., Cancer Statistics, 2021. *CA Cancer J Clin* **2021,** *71* (1), 7-33.

3. Siegel, R. L.; Miller, K. D.; Jemal, A., Cancer statistics, 2020. *CA Cancer J Clin* **2020,** *70* (1), 7-30.

4. Hammond, M. E.; Hayes, D. F.; Dowsett, M.; Allred, D. C.; Hagerty, K. L.; Badve, S.; Fitzgibbons, P. L.; Francis, G.; Goldstein, N. S.; Hayes, M.; Hicks, D. G.; Lester, S.; Love, R.; Mangu, P. B.; McShane, L.; Miller, K.; Osborne, C. K.; Paik, S.; Perlmutter, J.; Rhodes, A.; Sasano, H.; Schwartz, J. N.; Sweep, F. C.; Taube, S.; Torlakovic, E. E.; Valenstein, P.; Viale, G.; Visscher, D.; Wheeler, T.; Williams, R. B.; Wittliff, J. L.; Wolff, A. C., American Society of Clinical Oncology/College Of American Pathologists guideline recommendations for immunohistochemical testing of estrogen and progesterone receptors in breast cancer. *J Clin Oncol* **2010,** *28* (16), 2784-95.

5. Wolff, A. C.; Hammond, M. E.; Hicks, D. G.; Dowsett, M.; McShane, L. M.; Allison, K. H.; Allred, D. C.; Bartlett, J. M.; Bilous, M.; Fitzgibbons, P.; Hanna, W.; Jenkins, R. B.; Mangu, P. B.; Paik, S.; Perez, E. A.; Press, M. F.; Spears, P. A.; Vance, G. H.; Viale, G.; Hayes, D. F.; American Society of Clinical, O.; College of American, P., Recommendations for human epidermal growth factor receptor 2 testing in breast cancer: American Society of Clinical Oncology/College of American Pathologists clinical practice guideline update. *J Clin Oncol* **2013,** *31* (31), 3997-4013.

6. Manjunath, M.; Choudhary, B., Triple-negative breast cancer: A run-through of features, classification and current therapies. *Oncol Lett* **2021,** *22* (1), 512.

7. Won, K. A.; Spruck, C., Triple-negative breast cancer therapy: Current and future perspectives (Review). *Int J Oncol* **2020,** *57* (6), 1245-1261.

8. Almansour, N. M., Triple-Negative Breast Cancer: A Brief Review About Epidemiology, Risk Factors, Signaling Pathways, Treatment and Role of Artificial Intelligence. *Front Mol Biosci* **2022,** *9*, 836417.

9. Burguin, A.; Diorio, C.; Durocher, F., Breast Cancer Treatments: Updates and New Challenges. *J Pers Med* **2021,** *11* (8).

10. Yin, L.; Duan, J. J.; Bian, X. W.; Yu, S. C., Triple-negative breast cancer molecular subtyping and treatment progress. *Breast Cancer Res* **2020,** *22* (1), 61.

11. Fragomeni, S. M.; Sciallis, A.; Jeruss, J. S., Molecular Subtypes and Local-Regional Control of Breast Cancer. *Surg Oncol Clin N Am* **2018,** *27* (1), 95-120.

12. Hennigs, A.; Riedel, F.; Gondos, A.; Sinn, P.; Schirmacher, P.; Marme, F.; Jager, D.; Kauczor, H. U.; Stieber, A.; Lindel, K.; Debus, J.; Golatta, M.; Schutz, F.; Sohn, C.; Heil, J.; Schneeweiss, A., Prognosis of breast cancer molecular subtypes in routine clinical care: A large prospective cohort study. *BMC Cancer* **2016,** *16* (1), 734.

13. Li, Y.; Zhan, Z.; Yin, X.; Fu, S.; Deng, X., Targeted Therapeutic Strategies for Triple-Negative Breast Cancer. *Front Oncol* **2021,** *11*, 731535.

14. Won, K. A.; Spruck, C., Triplenegative breast cancer therapy: Current and future perspectives (Review). *Int J Oncol* **2020,** *57* (6), 1245-1261.

15. Singh, D. D.; Yadav, D. K., TNBC: Potential Targeting of Multiple Receptors for a Therapeutic Breakthrough, Nanomedicine, and Immunotherapy. *Biomedicines* **2021,** *9* (8).

16. Li, Y.; Zhang, H.; Merkher, Y.; Chen, L.; Liu, N.; Leonov, S.; Chen, Y., Recent advances in therapeutic strategies for triple-negative breast cancer. *J Hematol Oncol* **2022,** *15* (1), 121.

17. Salem, A. F.; Howell, A.; Sartini, M.; Sotgia, F.; Lisanti, M. P., Downregulation of stromal BRCA1 drives breast cancer tumor growth via upregulation of HIF-1alpha, autophagy and ketone body production. *Cell Cycle* **2012,** *11* (22), 4167-73.

18. Weil, M. K.; Chen, A. P., PARP inhibitor treatment in ovarian and breast cancer. *Curr Probl Cancer* **2011,** *35* (1), 7-50.

19. Gelmon, K. A.; Tischkowitz, M.; Mackay, H.; Swenerton, K.; Robidoux, A.; Tonkin, K.; Hirte, H.; Huntsman, D.; Clemons, M.; Gilks, B.; Yerushalmi, R.; Macpherson, E.; Carmichael, J.; Oza, A., Olaparib in patients with recurrent high-grade serous or poorly differentiated ovarian carcinoma or triple-negative breast cancer: a phase 2, multicentre, open-label, non-randomised study. *Lancet Oncol* **2011,** *12* (9), 852-61.

20. Jiang, Y. Z.; Liu, Y.; Xiao, Y.; Hu, X.; Jiang, L.; Zuo, W. J.; Ma, D.; Ding, J.; Zhu, X.; Zou, J.; Verschraegen, C.; Stover, D. G.; Kaklamani, V.; Wang, Z. H.; Shao, Z. M., Molecular subtyping and genomic profiling expand precision medicine in refractory metastatic triple-negative breast cancer: the FUTURE trial. *Cell Res* **2021,** *31* (2), 178-186.

21. Palfree, R. G., The urokinase-type plasminogen activator receptor is a member of the Ly-6 superfamily. *Immunol Today* **1991,** *12* (5), 170.

22. Stoppelli, M. P.; Corti, A.; Soffientini, A.; Cassani, G.; Blasi, F.; Assoian, R. K., Differentiation-enhanced binding of the amino-terminal fragment of human urokinase plasminogen activator to a specific receptor on U937 monocytes. *Proc Natl Acad Sci U S A* **1985,** *82* (15), 4939-43.

23. Vassalli, J. D.; Baccino, D.; Belin, D., A cellular binding site for the Mr 55,000 form of the human plasminogen activator, urokinase. *J Cell Biol* **1985,** *100* (1), 86-92.

24. Stephens, R. W.; Pollanen, J.; Tapiovaara, H.; Leung, K. C.; Sim, P. S.; Salonen, E. M.; Ronne, E.; Behrendt, N.; Dano, K.; Vaheri, A., Activation of pro-urokinase and plasminogen on human sarcoma cells: a proteolytic system with surface-bound reactants. *J Cell Biol* **1989,** *108* (5), 1987-95.

25. Lv, T.; Zhao, Y.; Jiang, X.; Yuan, H.; Wang, H.; Cui, X.; Xu, J.; Zhao, J.; Wang, J., uPAR: An Essential Factor for Tumor Development. *J Cancer* **2021,** *12* (23), 7026-7040.

26. Ossowski, L.; Clunie, G.; Masucci, M. T.; Blasi, F., In vivo paracrine interaction between urokinase and its receptor: effect on tumor cell invasion. *J Cell Biol* **1991,** *115* (4), 1107-12.

27. Smith, H. W.; Marshall, C. J., Regulation of cell signalling by uPAR. *Nat Rev Mol Cell Biol* **2010,** *11* (1), 23-36.

28. Tjwa, M.; Sidenius, N.; Moura, R.; Jansen, S.; Theunissen, K.; Andolfo, A.; De Mol, M.; Dewerchin, M.; Moons, L.; Blasi, F.; Verfaillie, C.; Carmeliet, P., Membrane-anchored uPAR regulates the proliferation, marrow pool size, engraftment, and mobilization of mouse hematopoietic stem/progenitor cells. *J Clin Invest* **2009,** *119* (4), 1008-18.

29. Huber, M. C.; Mall, R.; Braselmann, H.; Feuchtinger, A.; Molatore, S.; Lindner, K.; Walch, A.; Gross, E.; Schmitt, M.; Falkenberg, N.; Aubele, M., uPAR enhances malignant potential of triple-negative breast cancer by directly interacting with uPA and IGF1R. *BMC Cancer* **2016,** *16*, 615.

30. Giannopoulou, I.; Mylona, E.; Kapranou, A.; Mavrommatis, J.; Markaki, S.; Zoumbouli, C.; Keramopoulos, A.; Nakopoulou, L., The prognostic value of the topographic distribution of uPAR expression in invasive breast carcinomas. *Cancer Lett* **2007,** *246* (1-2), 262-7.

31. Zhai, B.-T.; Tian, H.; Sun, J.; Zou, J.-B.; Zhang, X.-F.; Cheng, J.-X.; Shi, Y.-J.; Fan, Y.; Guo, D.-Y., Urokinase-type plasminogen activator receptor (uPAR) as a therapeutic target in cancer. *Journal of Translational Medicine* **2022,** *20* (1), 135.

32. Gutova, M.; Najbauer, J.; Frank, R. T.; Kendall, S. E.; Gevorgyan, A.; Metz, M. Z.; Guevorkian, M.; Edmiston, M.; Zhao, D.; Glackin, C. A.; Kim, S. U.; Aboody, K. S., Urokinase plasminogen activator and urokinase plasminogen activator receptor mediate human stem cell tropism to malignant solid tumors. *Stem Cells* **2008,** *26* (6), 1406-13.

33. Yang, J. L.; Seetoo, D.; Wang, Y.; Ranson, M.; Berney, C. R.; Ham, J. M.; Russell, P. J.; Crowe, P. J., Urokinase-type plasminogen activator and its receptor in colorectal cancer: independent prognostic factors of metastasis and cancer-specific survival and potential therapeutic targets. *Int J Cancer* **2000,** *89* (5), 431-9.

34. Hildenbrand, R.; Wolf, G.; Bohme, B.; Bleyl, U.; Steinborn, A., Urokinase plasminogen activator receptor (CD87) expression of tumor-associated macrophages in ductal carcinoma in situ, breast cancer, and resident macrophages of normal breast tissue. *J Leukoc Biol* **1999,** *66* (1), 40-9.

35. Kim, S. J.; Shiba, E.; Taguchi, T.; Watanabe, T.; Tanji, Y.; Kimoto, Y.; Izukura, M.; Takai, S. I., Urokinase type plasminogen activator receptor is a novel prognostic factor in breast cancer. *Anticancer Res* **1997,** *17* (2B), 1373-8.

36. Wang, J.; Li, B.; Qiu, L.; Qiao, X.; Yang, H., Dendrimer-based drug delivery systems: history, challenges, and latest developments. *J Biol Eng* **2022,** *16* (1), 18.

37. Tomalia, D. A.; Baker, H.; Dewald, J.; Hall, M.; Kallos, G.; Martin, S.; Roeck, J.; Ryder, J.; Smith, P., A New Class of Polymers: Starburst-Dendritic Macromolecules. *Polymer Journal* **1985,** *17* (1), 117-132.

38. Patil, M. L.; Zhang, M.; Taratula, O.; Garbuzenko, O. B.; He, H.; Minko, T., Internally Cationic Polyamidoamine PAMAM-OH Dendrimers for siRNA Delivery: Effect of the Degree of Quaternization and Cancer Targeting. *Biomacromolecules* **2009,** *10* (2), 258-266.

39. Abedi-Gaballu, F.; Dehghan, G.; Ghaffari, M.; Yekta, R.; Abbaspour-Ravasjani, S.; Baradaran, B.; Dolatabadi, J. E. N.; Hamblin, M. R., PAMAM dendrimers as efficient drug and gene delivery nanosystems for cancer therapy. *Appl Mater Today* **2018,** *12*, 177-190.

40. Wang, J.; Li, B.; Qiu, L.; Qiao, X.; Yang, H., Dendrimer-based drug delivery systems: history, challenges, and latest developments. *Journal of Biological Engineering* **2022,** *16* (1), 18.

41. Parekh, H. S., The advance of dendrimers--a versatile targeting platform for gene/drug delivery. *Curr Pharm Des* **2007,** *13* (27), 2837-50.

42. Kurtoglu, Y. E.; Mishra, M. K.; Kannan, S.; Kannan, R. M., Drug release characteristics of PAMAM dendrimer-drug conjugates with different linkers. *Int J Pharm* **2010,** *384* (1-2), 189-94.

43. Dutta, K.; Das, R.; Medeiros, J.; Thayumanavan, S., Disulfide Bridging Strategies in Viral and Nonviral Platforms for Nucleic Acid Delivery. *Biochemistry* **2021,** *60* (13), 966-990.

44. Yang, H.; Morris, J. J.; Lopina, S. T., Polyethylene glycol-polyamidoamine dendritic micelle as solubility enhancer and the effect of the length of polyethylene glycol arms on the solubility of pyrene in water. *J Colloid Interface Sci* **2004,** *273* (1), 148-54.

45. Hamley, I. W., PEG-peptide conjugates. *Biomacromolecules* **2014,** *15* (5), 1543-59.

46. Liu, H.; Wang, H.; Yang, W.; Cheng, Y., Disulfide cross-linked low generation dendrimers with high gene transfection efficacy, low cytotoxicity, and low cost. *J Am Chem Soc* **2012,** *134* (42), 17680-7.

47. Dean, N. M.; Bennett, C. F., Antisense oligonucleotide-based therapeutics for cancer. *Oncogene* **2003,** *22* (56), 9087-96.

48. Lee, Y.; Vassilakos, A.; Feng, N.; Lam, V.; Xie, H.; Wang, M.; Jin, H.; Xiong, K.; Liu, C.; Wright, J.; Young, A., GTI-2040, an antisense agent targeting the small subunit component (R2) of human ribonucleotide reductase, shows potent antitumor activity against a variety of tumors. *Cancer Res* **2003,** *63* (11), 2802-11.

49. Dhuri, K.; Bechtold, C.; Quijano, E.; Pham, H.; Gupta, A.; Vikram, A.; Bahal, R., Antisense Oligonucleotides: An Emerging Area in Drug Discovery and Development. *J Clin Med* **2020,** *9* (6).

50. Furdon, P. J.; Dominski, Z.; Kole, R., RNase H cleavage of RNA hybridized to oligonucleotides containing methylphosphonate, phosphorothioate and phosphodiester bonds. *Nucleic Acids Res* **1989,** *17* (22), 9193-204.

51. Jordan, A.; Reichard, P., Ribonucleotide reductases. *Annu Rev Biochem* **1998,** *67*, 71-98.

52. Nordlund, P.; Reichard, P., Ribonucleotide reductases. *Annu Rev Biochem* **2006,** *75*, 681-706.

53. Kolberg, M.; Strand, K. R.; Graff, P.; Andersson, K. K., Structure, function, and mechanism of ribonucleotide reductases. *Biochim Biophys Acta* **2004,** *1699* (1-2), 1-34.

54. Elford, H. L.; Freese, M.; Passamani, E.; Morris, H. P., Ribonucleotide reductase and cell proliferation. I. Variations of ribonucleotide reductase activity with tumor growth rate in a series of rat hepatomas. *J Biol Chem* **1970,** *245* (20), 5228-33.

55. Abdel-Rahman, M. A.; Mahfouz, M.; Habashy, H. O., RRM2 expression in different molecular subtypes of breast cancer and its prognostic significance. *Diagn Pathol* **2022,** *17* (1), 1.

56. Wilson, E. A.; Elford, H. L.; Faridi, J. S., 272 - The Role of Ribonucleotide Reductase (RR) in Breast Cancer and the Therapeutic Potential of the RR Inhibitor Didox. *Free Radical Biology and Medicine* **2016,** *100*, S121.

57. Aye, Y.; Li, M.; Long, M. J.; Weiss, R. S., Ribonucleotide reductase and cancer: biological mechanisms and targeted therapies. *Oncogene* **2015,** *34* (16), 2011-21.

58. Shao, J.; Liu, X.; Zhu, L.; Yen, Y., Targeting ribonucleotide reductase for cancer therapy. *Expert Opin Ther Targets* **2013,** *17* (12), 1423-37.

59. Zhang, H.; Liu, X.; Warden, C. D.; Huang, Y.; Loera, S.; Xue, L.; Zhang, S.; Chu, P.; Zheng, S.; Yen, Y., Prognostic and therapeutic significance of ribonucleotide reductase small subunit M2 in estrogen-negative breast cancers. *BMC Cancer* **2014,** *14*, 664.

60. Zuo, Z.; Zhou, Z.; Chang, Y.; Liu, Y.; Shen, Y.; Li, Q.; Zhang, L., Ribonucleotide reductase M2 (RRM2): Regulation, function and targeting strategy in human cancer. *Genes Dis* **2024,** *11* (1), 218-233.

61. Shao, J.; Zhou, B.; Chu, B.; Yen, Y., Ribonucleotide reductase inhibitors and future drug design. *Curr Cancer Drug Targets* **2006,** *6* (5), 409-31.

62. Li, J.; Pang, J.; Liu, Y.; Zhang, J.; Zhang, C.; Shen, G.; Song, L., Suppression of RRM2 inhibits cell proliferation, causes cell cycle arrest and promotes the apoptosis of human neuroblastoma cells and in human neuroblastoma RRM2 is suppressed following chemotherapy. *Oncol Rep* **2018,** *40* (1), 355-360.

63. Zhan, Y.; Jiang, L.; Jin, X.; Ying, S.; Wu, Z.; Wang, L.; Yu, W.; Tong, J.; Zhang, L.; Lou, Y.; Qiu, Y., Inhibiting RRM2 to enhance the anticancer activity of chemotherapy. *Biomed Pharmacother* **2021,** *133*, 110996.

64. Mannargudi, M. B.; Deb, S., Clinical pharmacology and clinical trials of ribonucleotide reductase inhibitors: is it a viable cancer therapy? *J Cancer Res Clin Oncol* **2017,** *143* (8), 1499-1529.

65. Davis, M. E., The first targeted delivery of siRNA in humans via a self-assembling, cyclodextrin polymer-based nanoparticle: from concept to clinic. *Mol Pharm* **2009,** *6* (3), 659-68.

66. Zuckerman, J. E.; Gritli, I.; Tolcher, A.; Heidel, J. D.; Lim, D.; Morgan, R.; Chmielowski, B.; Ribas, A.; Davis, M. E.; Yen, Y., Correlating animal and human phase Ia/Ib clinical data with CALAA-01, a targeted, polymer-based nanoparticle containing siRNA. *Proc Natl Acad Sci U S A* **2014,** *111* (31), 11449-54.

67. Orr, R. M., GTI-2040. Lorus Therapeutics. *Curr Opin Investig Drugs* **2001,** *2* (10), 1462-6.

68. Juhasz, A.; Vassilakos, A.; Chew, H. K.; Gandara, D.; Yen, Y., Analysis of ribonucleotide reductase M2 mRNA levels in patient samples after GTI-2040 antisense drug treatment. *Oncol Rep* **2006,** *15* (5), 1299-304.

69. Eckstein, F., Phosphorothioates, essential components of therapeutic oligonucleotides. *Nucleic Acid Ther* **2014,** *24* (6), 374-87.

70. Putney, S. D.; Benkovic, S. J.; Schimmel, P. R., A DNA fragment with an alpha-phosphorothioate nucleotide at one end is asymmetrically blocked from digestion by exonuclease III and can be replicated in vivo. *Proc Natl Acad Sci U S A* **1981,** *78* (12), 7350-4.

71. Klisovic, R. B.; Blum, W.; Liu, Z.; Xie, Z.; Kefauver, C.; Huynh, L.; Zwiebel, J. A.; Devine, S. M.; Byrd, J. C.; Grever, M. R.; Chan, K. K.; Marcucci, G., Phase I study of GTI-2040, a ribonucleotide reductase antisense, with high dose cytarabine in patients with relapsed/refractory acute myeloid leukemia. *Leuk Lymphoma* **2014,** *55* (6), 1332-6.

72. Malik, L.; Zwiebel, A.; Cooper, J., A phase I pharmacokinetic and pharmacodynamic study of GTI-2040 in combination with gemcitabine in patients with solid tumors. *Cancer Chemother Pharmacol* **2018,** *82* (3), 533-539.

73. Stadler, W. M.; Desai, A. A.; Quinn, D. I.; Bukowski, R.; Poiesz, B.; Kardinal, C. G.; Lewis, N.; Makalinao, A.; Murray, P.; Torti, F. M., A Phase I/II study of GTI-2040 and capecitabine in patients with renal cell carcinoma. *Cancer Chemother Pharmacol* **2008,** *61* (4), 689-94.

74. Desai, A. A.; Schilsky, R. L.; Young, A.; Janisch, L.; Stadler, W. M.; Vogelzang, N. J.; Cadden, S.; Wright, J. A.; Ratain, M. J., A phase I study of antisense oligonucleotide GTI-2040 given by continuous intravenous infusion in patients with advanced solid tumors. *Ann Oncol* **2005,** *16* (6), 958-65.

75. Klisovic, R. B.; Blum, W.; Wei, X.; Liu, S.; Liu, Z.; Xie, Z.; Vukosavljevic, T.; Kefauver, C.; Huynh, L.; Pang, J.; Zwiebel, J. A.; Devine, S.; Byrd, J. C.; Grever, M. R.; Chan, K.; Marcucci, G., Phase I study of GTI-2040, an antisense to ribonucleotide reductase, in combination with high-dose cytarabine in patients with acute myeloid leukemia. *Clin Cancer Res* **2008,** *14* (12), 3889-95.

76. Leighl, N. B.; Laurie, S. A.; Chen, X. E.; Ellis, P.; Shepherd, F. A.; Knox, J. J.; Goss, G.; Burkes, R. L.; Pond, G. R.; Dick, C.; Yen, Y.; Zwiebel, J. A.; Moore, M. J., A phase I/II study of GTI-2040 plus docetaxel as second-line treatment in advanced non-small cell lung cancer: a study of the PMH phase II consortium. *J Thorac Oncol* **2009,** *4* (9), 1163-9.

77. Shibata, S. I.; Doroshow, J. H.; Frankel, P.; Synold, T. W.; Yen, Y.; Gandara, D. R.; Lenz, H. J.; Chow, W. A.; Leong, L. A.; Lim, D.; Margolin, K. A.; Morgan, R. J.; Somlo, G.; Newman, E. M., Phase I trial of GTI-2040, oxaliplatin, and capecitabine in the treatment of advanced metastatic solid tumors: a California Cancer Consortium Study. *Cancer Chemother Pharmacol* **2009,** *64* (6), 1149-55.

78. Sridhar, S. S.; Canil, C. M.; Chi, K. N.; Hotte, S. J.; Ernst, S.; Wang, L.; Chen, E. X.; Juhasz, A.; Yen, Y.; Murray, P.; Zwiebel, J. A.; Moore, M. J., A phase II study of the antisense oligonucleotide GTI-2040 plus docetaxel and prednisone as first-line treatment in castration-resistant prostate cancer. *Cancer Chemother Pharmacol* **2011,** *67* (4), 927-33.

79. Madler, S.; Bich, C.; Touboul, D.; Zenobi, R., Chemical cross-linking with NHS esters: a systematic study on amino acid reactivities. *J Mass Spectrom* **2009,** *44* (5), 694-706.

80. Rennick, J. J.; Johnston, A. P. R.; Parton, R. G., Key principles and methods for studying the endocytosis of biological and nanoparticle therapeutics. *Nature Nanotechnology* **2021,** *16* (3), 266-276.

81. Daniel, J. A.; Chau, N.; Abdel-Hamid, M. K.; Hu, L.; von Kleist, L.; Whiting, A.; Krishnan, S.; Maamary, P.; Joseph, S. R.; Simpson, F.; Haucke, V.; McCluskey, A.; Robinson, P. J., Phenothiazine-derived antipsychotic drugs inhibit dynamin and clathrin-mediated endocytosis. *Traffic* **2015,** *16* (6), 635-54.

82. Wang, L. H.; Rothberg, K. G.; Anderson, R. G., Mis-assembly of clathrin lattices on endosomes reveals a regulatory switch for coated pit formation. *J Cell Biol* **1993,** *123* (5), 1107-17.

83. Bolard, J., How do the polyene macrolide antibiotics affect the cellular membrane properties? *Biochim Biophys Acta* **1986,** *864* (3-4), 257-304.

84. Gladhaug, I. P.; Christoffersen, T., Amiloride inhibits constitutive internalization and increases the surface number of epidermal growth factor receptors in intact rat hepatocytes. *J Cell Physiol* **1990,** *143* (1), 188-95.

85. Kleyman, T. R.; Cragoe, E. J., Jr., Amiloride and its analogs as tools in the study of ion transport. *J Membr Biol* **1988,** *105* (1), 1-21.

86. Lim, H. K.; Lee, H.; Moon, A.; Kang, K.-T.; Jung, J. J. T. C. R., Exploring protocol for breast cancer xenograft model using endothelial colony-forming cells. **2018,** *7* (5), 1228-1234.

87. Saito, G.; Swanson, J. A.; Lee, K. D., Drug delivery strategy utilizing conjugation via reversible disulfide linkages: role and site of cellular reducing activities. *Adv Drug Deliv Rev* **2003,** *55* (2), 199-215.

88. Schafer, F. Q.; Buettner, G. R., Redox environment of the cell as viewed through the redox state of the glutathione disulfide/glutathione couple. *Free Radic Biol Med* **2001,** *30* (11), 1191-212.

89. Poole, L. B., The basics of thiols and cysteines in redox biology and chemistry. *Free Radic Biol Med* **2015,** *80*, 148-57.

90. Justus, C. R.; Dong, L.; Yang, L. V., Acidic tumor microenvironment and pH-sensing G protein-coupled receptors. *Front Physiol* **2013,** *4*, 354.

91. Uthaman, S.; Huh, K. M.; Park, I. K., Tumor microenvironment-responsive nanoparticles for cancer theragnostic applications. *Biomater Res* **2018,** *22*, 22.

92. Boussif, O.; Lezoualc'h, F.; Zanta, M. A.; Mergny, M. D.; Scherman, D.; Demeneix, B.; Behr, J. P., A versatile vector for gene and oligonucleotide transfer into cells in culture and in vivo: polyethylenimine. *Proc Natl Acad Sci U S A* **1995,** *92* (16), 7297-301.

93. Gunti, S.; Hoke, A. T. K.; Vu, K. P.; London, N. R., Jr., Organoid and Spheroid Tumor Models: Techniques and Applications. *Cancers (Basel)* **2021,** *13* (4).

94. Barua, S.; Mitragotri, S., Challenges associated with Penetration of Nanoparticles across Cell and Tissue Barriers: A Review of Current Status and Future Prospects. *Nano Today* **2014,** *9* (2), 223-243.

95. Keller, A.; Linko, V., Challenges and Perspectives of DNA Nanostructures in Biomedicine. *Angew Chem Int Ed Engl* **2020,** *59* (37), 15818-15833.

96. Forman, H. J.; Zhang, H.; Rinna, A., Glutathione: overview of its protective roles, measurement, and biosynthesis. *Mol Aspects Med* **2009,** *30* (1-2), 1-12.

97. Shan, J.; Wang, Z.; Mo, Q.; Long, J.; Fan, Y.; Cheng, L.; Zhang, T.; Liu, X.; Wang, X., Ribonucleotide reductase M2 subunit silencing suppresses tumorigenesis in pancreatic cancer via inactivation of PI3K/AKT/mTOR pathway. *Pancreatology* **2022,** *22* (3), 401-413.

98. Li, S.; Mai, H.; Zhu, Y.; Li, G.; Sun, J.; Li, G.; Liang, B.; Chen, S., MicroRNA-4500 Inhibits Migration, Invasion, and Angiogenesis of Breast Cancer Cells via RRM2-Dependent MAPK Signaling Pathway. *Mol Ther Nucleic Acids* **2020,** *21*, 278-289.

99. Zhuang, S.; Li, L.; Zang, Y.; Li, G.; Wang, F., RRM2 elicits the metastatic potential of breast cancer cells by regulating cell invasion, migration and VEGF expression via the PI3K/AKT signaling. *Oncol Lett* **2020,** *19* (4), 3349-3355.

100. Wang, N.; Li, Y.; Zhou, J., Downregulation of ribonucleotide reductase subunits M2 induces apoptosis and G1 arrest of cervical cancer cells. *Oncol Lett* **2018,** *15* (3), 3719-3725.

101. Rahman, M. A.; Amin, A. R.; Wang, D.; Koenig, L.; Nannapaneni, S.; Chen, Z.; Wang, Z.; Sica, G.; Deng, X.; Chen, Z. G.; Shin, D. M., RRM2 regulates Bcl-2 in head and neck and lung cancers: a potential target for cancer therapy. *Clin Cancer Res* **2013,** *19* (13), 3416-28.

102. Grusch, M.; Fritzer-Szekeres, M.; Fuhrmann, G.; Rosenberger, G.; Luxbacher, C.; Elford, H. L.; Smid, K.; Peters, G. J.; Szekeres, T.; Krupitza, G., Activation of caspases and induction of apoptosis by novel ribonucleotide reductase inhibitors amidox and didox. *Exp Hematol* **2001,** *29* (5), 623-32.

103. Xia, G.; Wang, H.; Song, Z.; Meng, Q.; Huang, X.; Huang, X., Gambogic acid sensitizes gemcitabine efficacy in pancreatic cancer by reducing the expression of ribonucleotide reductase subunit-M2 (RRM2). *J Exp Clin Cancer Res* **2017,** *36* (1), 107.

SECTION

2. CONCLUSION

This thesis demonstrates that this GDP-uPA has great potential to become an efficient targeted delivery system to improve the therapeutic effectiveness of GTI for TNBC treatment. Enhanced R2 knockdown can be achieved by GDP-uPA/GTI in TNBC model through its better delivery of GTI, tumor-targeted capacity, and increased penetration and retention in tumor.

GDP-uPA can also carry various anti-cancer nucleic acids (e.g., siRNA/miRNA/plasmid/antisense oligonucleotide) and be applied to other types of cancer with high uPAR level including TNBC. Besides, the strategy of utilizing uPA binding domain as a targeted ligand can be practiced with different kinds of vehicles such as liposomes and lipid nanoparticles for diverse usages in cancer therapies. It is expected that this thesis can bring us more knowledge of possible therapies with GDP-uPA in uPAR highly expressed cancers including TNBC and benefit more patients

APPENDIX

ADDITIONAL FIGURES FROM PAPER I

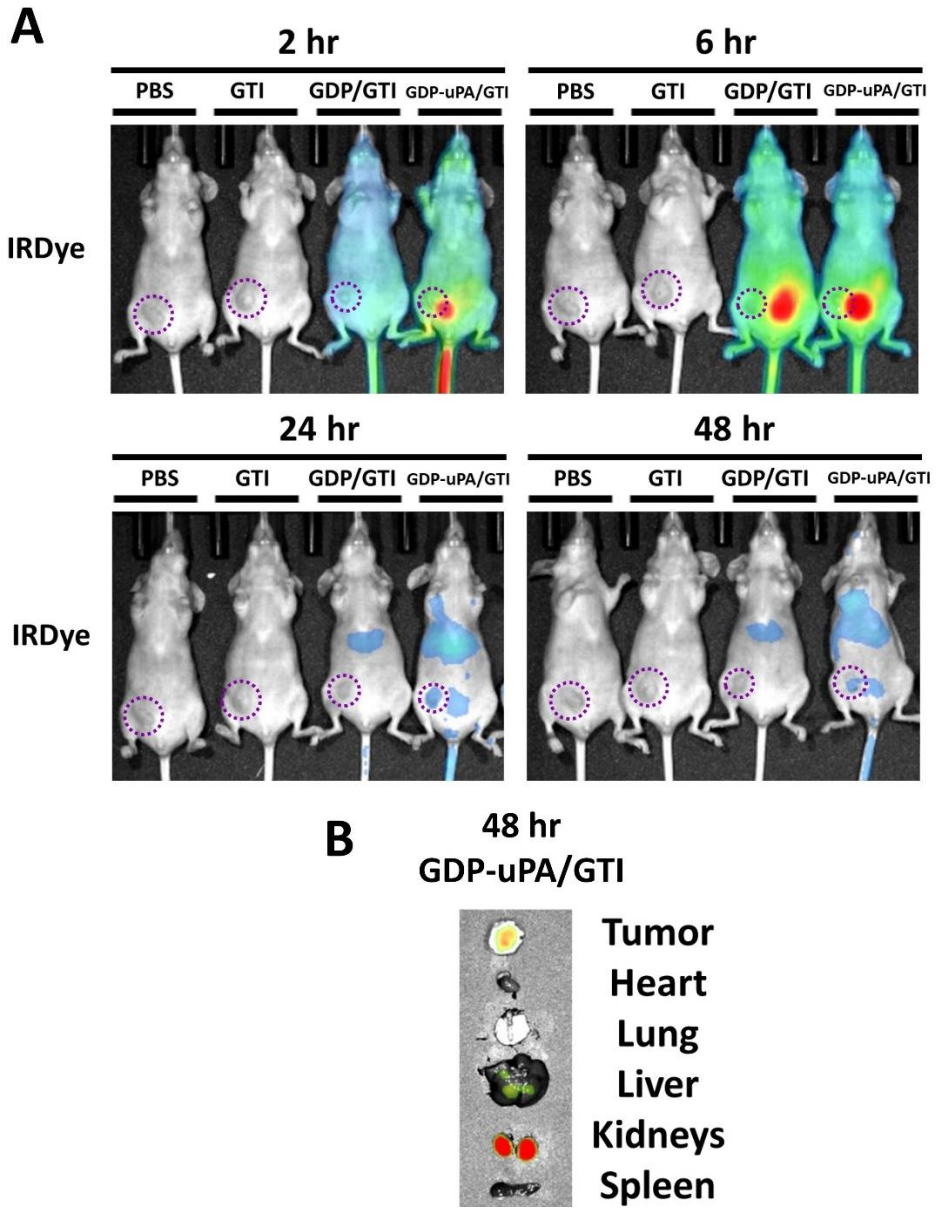

Figure A1. Biodistribution studies of PBS, GTI, GDP/GTI, and GDP-uPA/GTI in an TNBC xenograft model with older age. (A) Whole body and (B) tumor and organs images taken by AMI HTX imaging system. Purple circle: tumor site.

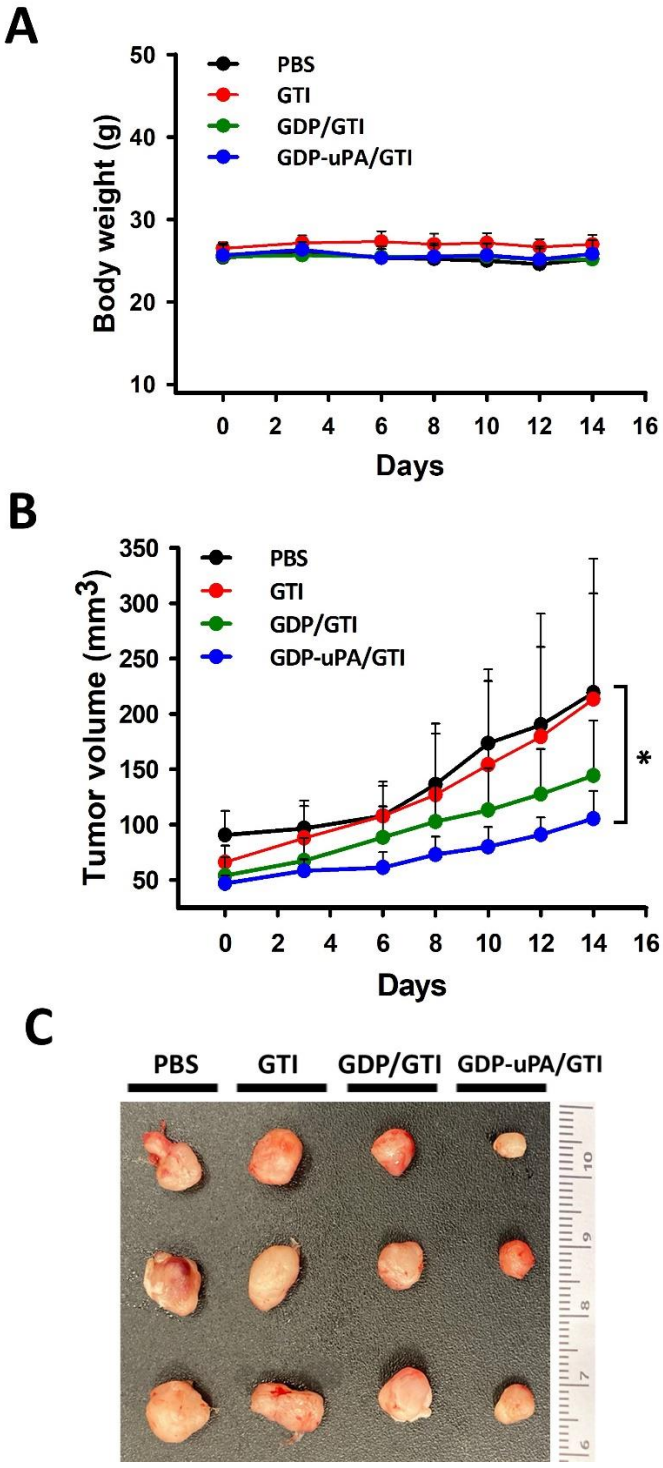

Figure A2. Therapeutic studies of PBS, GTI, GDP/GTI, and GDP-uPA/GTI in a TNBC xenograft model with older age. (A) Body weight and (B) tumor volume were monitored during the administration duration. (C) Tumors were collected after elimination of mice. Data are shown as mean ± SD (n=5~6). *: $p < 0.05$, compared with the PBS group.

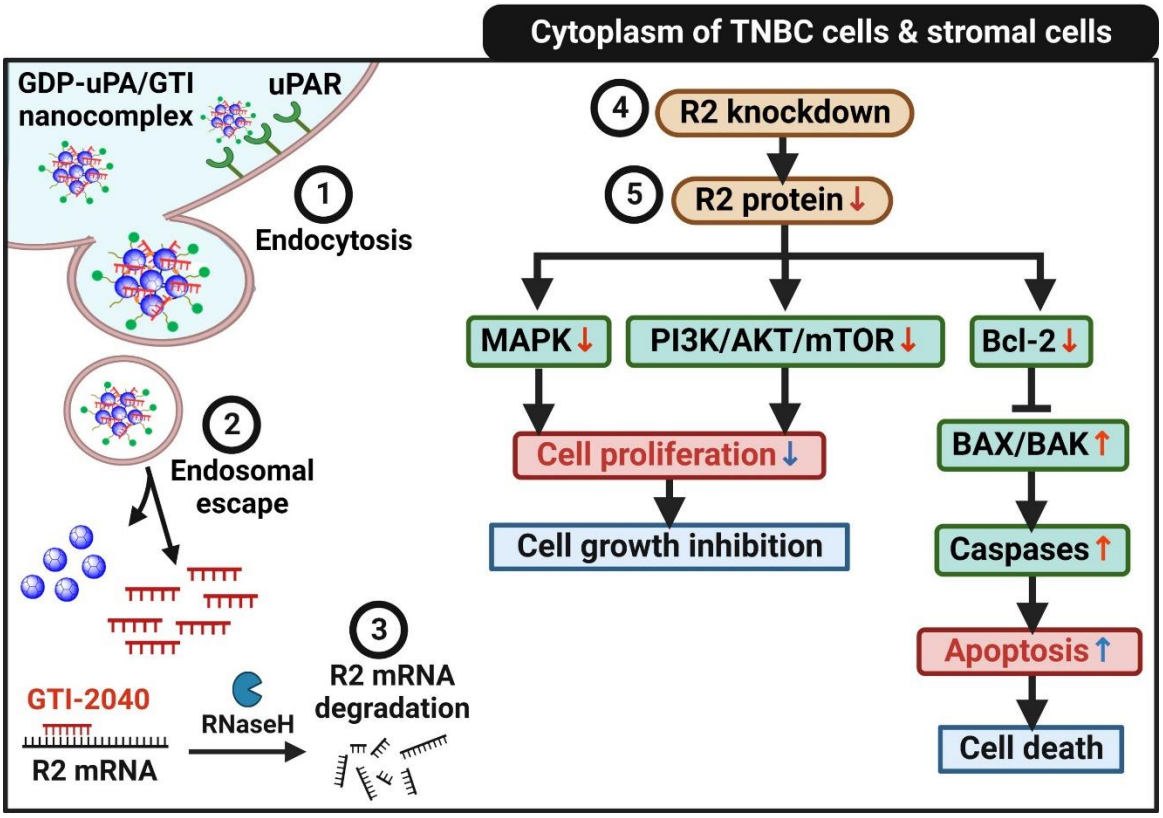

Figure A3. A schematic diagram of the proposed future direction. The TNBC xenograft model is used to evaluate the tumor suppression resulting from enhanced R2 knockdown by our GDP-uPA/GTI nanocomplex and identify the signaling pathways regulated by the enhanced R2 knockdown. GDP-uPA/GTI nanostructure is our strategy to explore the mechanisms of R2 knockdown in TNBC tumor suppression. GDP-uPA/GTI is proposed to distribute to uPAR highly expressed tumor site through blood stream due to its uPA targeting ligand. After being taken by TNBC cells and cancer-associated stromal cells via endocytosis, GTI-2040 (GTI) can be released from GDP-uPA/GTI complex and knockdown human R2 mRNA in cytoplasm, which leads to reduced level of R2 protein and further results in cell death. The effects of R2 knockdown on cell proliferation-related pathways (e.g., MAPK, PI3K/AKT/mTOR), and apoptosis-related pathways (e.g., Bcl-2, BAX/BAK, caspases) are proposed to assess by ELISA assays. R2: ribonucleotide reductase β2 subunit. GDP-uPA/GTI: G2-DSP-PEG-uPA carrying GTI; GTI: an antisense oligonucleotide of human R2 mRNA.

BIBLIOGRAPHY

1. Siegel, R. L.; Miller, K. D.; Fuchs, H. E.; Jemal, A., Cancer statistics, 2022. CA Cancer J Clin 2022, 72 (1), 7-33.

2. Siegel, R. L.; Miller, K. D.; Fuchs, H. E.; Jemal, A., Cancer Statistics, 2021. CA Cancer J Clin 2021, 71 (1), 7-33.

3. Siegel, R. L.; Miller, K. D.; Jemal, A., Cancer statistics, 2020. CA Cancer J Clin 2020, 70 (1), 7-30.

4. Orrantia-Borunda, E.; Anchondo-Nunez, P.; Acuna-Aguilar, L. E.; Gomez-Valles, F. O.; Ramirez-Valdespino, C. A., Subtypes of Breast Cancer. In Breast Cancer, Mayrovitz, H. N., Ed. Brisbane (AU), 2022.

5. Inwald, E. C.; Koller, M.; Klinkhammer-Schalke, M.; Zeman, F.; Hofstadter, F.; Gerstenhauer, M.; Brockhoff, G.; Ortmann, O., 4-IHC classification of breast cancer subtypes in a large cohort of a clinical cancer registry: use in clinical routine for therapeutic decisions and its effect on survival. Breast Cancer Res Treat 2015, 153 (3), 647-58.

6. Yeh, I. T.; Mies, C., Application of immunohistochemistry to breast lesions. Arch Pathol Lab Med 2008, 132 (3), 349-58.

7. Yin, L.; Duan, J. J.; Bian, X. W.; Yu, S. C., Triple-negative breast cancer molecular subtyping and treatment progress. Breast Cancer Res 2020, 22 (1), 61.

8. Hammond, M. E.; Hayes, D. F.; Dowsett, M.; Allred, D. C.; Hagerty, K. L.; Badve, S.; Fitzgibbons, P. L.; Francis, G.; Goldstein, N. S.; Hayes, M.; Hicks, D. G.; Lester, S.; Love, R.; Mangu, P. B.; McShane, L.; Miller, K.; Osborne, C. K.; Paik, S.; Perlmutter, J.; Rhodes, A.; Sasano, H.; Schwartz, J. N.; Sweep, F. C.; Taube, S.; Torlakovic, E. E.; Valenstein, P.; Viale, G.; Visscher, D.; Wheeler, T.; Williams, R. B.; Wittliff, J. L.; Wolff, A. C., American Society of Clinical Oncology/College Of American Pathologists guideline recommendations for immunohistochemical testing of estrogen and progesterone receptors in breast cancer. J Clin Oncol 2010, 28 (16), 2784-95.

9. Wolff, A. C.; Hammond, M. E.; Hicks, D. G.; Dowsett, M.; McShane, L. M.; Allison, K. H.; Allred, D. C.; Bartlett, J. M.; Bilous, M.; Fitzgibbons, P.; Hanna, W.; Jenkins, R. B.; Mangu, P. B.; Paik, S.; Perez, E. A.; Press, M. F.; Spears, P. A.; Vance, G. H.; Viale, G.; Hayes, D. F.; American Society of Clinical, O.; College of American, P., Recommendations for human epidermal growth factor receptor 2 testing in breast cancer: American Society of Clinical Oncology/College of American Pathologists clinical practice guideline update. J Clin Oncol 2013, 31 (31), 3997-4013.

10. Manjunath, M.; Choudhary, B., Triple-negative breast cancer: A run-through of features, classification and current therapies. Oncol Lett 2021, 22 (1), 512.

11. Won, K. A.; Spruck, C., Triple-negative breast cancer therapy: Current and future perspectives (Review). Int J Oncol 2020, 57 (6), 1245-1261.

12. Almansour, N. M., Triple-Negative Breast Cancer: A Brief Review About Epidemiology, Risk Factors, Signaling Pathways, Treatment and Role of Artificial Intelligence. Front Mol Biosci 2022, 9, 836417.

13. Rouzier, R.; Perou, C. M.; Symmans, W. F.; Ibrahim, N.; Cristofanilli, M.; Anderson, K.; Hess, K. R.; Stec, J.; Ayers, M.; Wagner, P.; Morandi, P.; Fan, C.; Rabiul, I.; Ross, J. S.; Hortobagyi, G. N.; Pusztai, L., Breast cancer molecular subtypes respond differently to preoperative chemotherapy. Clin Cancer Res 2005, 11 (16), 5678-85.

14. Voduc, K. D.; Cheang, M. C.; Tyldesley, S.; Gelmon, K.; Nielsen, T. O.; Kennecke, H., Breast cancer subtypes and the risk of local and regional relapse. J Clin Oncol 2010, 28 (10), 1684-91.

15. Soerjomataram, I.; Louwman, M. W.; Ribot, J. G.; Roukema, J. A.; Coebergh, J. W., An overview of prognostic factors for long-term survivors of breast cancer. Breast Cancer Res Treat 2008, 107 (3), 309-30.

16. Shen, Y.; Yang, Y.; Inoue, L. Y.; Munsell, M. F.; Miller, A. B.; Berry, D. A., Role of detection method in predicting breast cancer survival: analysis of randomized screening trials. J Natl Cancer Inst 2005, 97 (16), 1195-203.

17. Howlader, N.; Cronin, K. A.; Kurian, A. W.; Andridge, R., Differences in Breast Cancer Survival by Molecular Subtypes in the United States. Cancer Epidemiol Biomarkers Prev 2018, 27 (6), 619-626.

18. Dong, G.; Wang, D.; Liang, X.; Gao, H.; Wang, L.; Yu, X.; Liu, J., Factors related to survival rates for breast cancer patients. Int J Clin Exp Med 2014, 7 (10), 3719-24.

19. Fleege, N. M. G.; Cobain, E. F. J. B. P.; Obstetrics, R. C.; Gynaecology, Breast cancer management in 2021: A primer for the obstetrics and gynecology. 2022, 82, 30-45.

20. Lukasiewicz, S.; Czeczelewski, M.; Forma, A.; Baj, J.; Sitarz, R.; Stanislawek, A., Breast Cancer-Epidemiology, Risk Factors, Classification, Prognostic Markers, and Current Treatment Strategies-An Updated Review. Cancers (Basel) 2021, 13 (17).

21. Jacobs, A. T.; Martinez Castaneda-Cruz, D.; Rose, M. M.; Connelly, L., Targeted therapy for breast cancer: An overview of drug classes and outcomes. Biochem Pharmacol 2022, 204, 115209.

22. Morris, G. J.; Naidu, S.; Topham, A. K.; Guiles, F.; Xu, Y.; McCue, P.; Schwartz, G. F.; Park, P. K.; Rosenberg, A. L.; Brill, K.; Mitchell, E. P., Differences in breast carcinoma characteristics in newly diagnosed African-American and Caucasian patients: a single-institution compilation compared with the National Cancer Institute's Surveillance, Epidemiology, and End Results database. Cancer 2007, 110 (4), 876-84.

23. Plasilova, M. L.; Hayse, B.; Killelea, B. K.; Horowitz, N. R.; Chagpar, A. B.; Lannin, D. R., Features of triple-negative breast cancer: Analysis of 38,813 cases from the national cancer database. Medicine (Baltimore) 2016, 95 (35), e4614.

24. Dent, R.; Trudeau, M.; Pritchard, K. I.; Hanna, W. M.; Kahn, H. K.; Sawka, C. A.; Lickley, L. A.; Rawlinson, E.; Sun, P.; Narod, S. A., Triple-negative breast cancer: clinical features and patterns of recurrence. Clin Cancer Res 2007, 13 (15 Pt 1), 4429-34.

25. do Nascimento, R. G.; Otoni, K. M. J. M., Histological and molecular classification of breast cancer: what do we know? 2020, 30, 1-8.

26. Waks, A. G.; Winer, E. P., Breast Cancer Treatment: A Review. JAMA 2019, 321 (3), 288-300.

27. Caparica, R.; Lambertini, M.; de Azambuja, E., How I treat metastatic triple-negative breast cancer. ESMO Open 2019, 4, e000504.

28. O'Reilly, D.; Sendi, M. A.; Kelly, C. M., Overview of recent advances in metastatic triple negative breast cancer. World J Clin Oncol 2021, 12 (3), 164-182.

29. Yao, Y.; Chu, Y.; Xu, B.; Hu, Q.; Song, Q., Risk factors for distant metastasis of patients with primary triple-negative breast cancer. Biosci Rep 2019, 39 (6).

30. Li, Y.; Zhan, Z.; Yin, X.; Fu, S.; Deng, X., Targeted Therapeutic Strategies for Triple-Negative Breast Cancer. Front Oncol 2021, 11, 731535.

31. Won, K. A.; Spruck, C., Triplenegative breast cancer therapy: Current and future perspectives (Review). Int J Oncol 2020, 57 (6), 1245-1261.

32. Singh, D. D.; Yadav, D. K., TNBC: Potential Targeting of Multiple Receptors for a Therapeutic Breakthrough, Nanomedicine, and Immunotherapy. Biomedicines 2021, 9 (8).

33. Li, Y.; Zhang, H.; Merkher, Y.; Chen, L.; Liu, N.; Leonov, S.; Chen, Y., Recent advances in therapeutic strategies for triple-negative breast cancer. J Hematol Oncol 2022, 15 (1), 121.

34. Jiang, Y. Z.; Liu, Y.; Xiao, Y.; Hu, X.; Jiang, L.; Zuo, W. J.; Ma, D.; Ding, J.; Zhu, X.; Zou, J.; Verschraegen, C.; Stover, D. G.; Kaklamani, V.; Wang, Z. H.; Shao, Z. M., Molecular subtyping and genomic profiling expand precision medicine in refractory metastatic triple-negative breast cancer: the FUTURE trial. Cell Res 2021, 31 (2), 178-186.

35. Gelmon, K. A.; Tischkowitz, M.; Mackay, H.; Swenerton, K.; Robidoux, A.; Tonkin, K.; Hirte, H.; Huntsman, D.; Clemons, M.; Gilks, B.; Yerushalmi, R.; Macpherson, E.; Carmichael, J.; Oza, A., Olaparib in patients with recurrent high-grade serous or poorly differentiated ovarian carcinoma or triple-negative breast cancer: a phase 2, multicentre, open-label, non-randomised study. Lancet Oncol 2011, 12 (9), 852-61.

36. Kong, X.; Qi, Y.; Wang, X.; Jiang, R.; Wang, J.; Fang, Y.; Gao, J.; Chu Hwang, K., Nanoparticle drug delivery systems and their applications as targeted therapies for triple negative breast cancer. Progress in Materials Science 2023, 134, 101070.

37. Thakur, V.; Kutty, R. V., Recent advances in nanotheranostics for triple negative breast cancer treatment. J Exp Clin Cancer Res 2019, 38 (1), 430.

38. Golombek, S. K.; May, J. N.; Theek, B.; Appold, L.; Drude, N.; Kiessling, F.; Lammers, T., Tumor targeting via EPR: Strategies to enhance patient responses. Adv Drug Deliv Rev 2018, 130, 17-38.

39. Hossein-Nejad-Ariani, H.; Althagafi, E.; Kaur, K., Small Peptide Ligands for Targeting EGFR in Triple Negative Breast Cancer Cells. Sci Rep 2019, 9 (1), 2723.

40. Nabil, G.; Alzhrani, R.; Alsaab, H. O.; Atef, M.; Sau, S.; Iyer, A. K.; Banna, H. E., CD44 Targeted Nanomaterials for Treatment of Triple-Negative Breast Cancer. Cancers (Basel) 2021, 13 (4).

41. Wang, J.; Li, B.; Qiu, L.; Qiao, X.; Yang, H., Dendrimer-based drug delivery systems: history, challenges, and latest developments. J Biol Eng 2022, 16 (1), 18.

42. Tomalia, D. A.; Baker, H.; Dewald, J.; Hall, M.; Kallos, G.; Martin, S.; Roeck, J.; Ryder, J.; Smith, P., A New Class of Polymers: Starburst-Dendritic Macromolecules. Polymer Journal 1985, 17 (1), 117-132.

43. Patil, M. L.; Zhang, M.; Taratula, O.; Garbuzenko, O. B.; He, H.; Minko, T., Internally Cationic Polyamidoamine PAMAM-OH Dendrimers for siRNA Delivery: Effect of the Degree of Quaternization and Cancer Targeting. Biomacromolecules 2009, 10 (2), 258-266.

44. Abedi-Gaballu, F.; Dehghan, G.; Ghaffari, M.; Yekta, R.; Abbaspour-Ravasjani, S.; Baradaran, B.; Dolatabadi, J. E. N.; Hamblin, M. R., PAMAM dendrimers as efficient drug and gene delivery nanosystems for cancer therapy. Appl Mater Today 2018, 12, 177-190.

45. Huber, M. C.; Mall, R.; Braselmann, H.; Feuchtinger, A.; Molatore, S.; Lindner, K.; Walch, A.; Gross, E.; Schmitt, M.; Falkenberg, N.; Aubele, M., uPAR enhances malignant potential of triple-negative breast cancer by directly interacting with uPA and IGF1R. BMC Cancer 2016, 16, 615.

46. Giannopoulou, I.; Mylona, E.; Kapranou, A.; Mavrommatis, J.; Markaki, S.; Zoumbouli, C.; Keramopoulos, A.; Nakopoulou, L., The prognostic value of the topographic distribution of uPAR expression in invasive breast carcinomas. Cancer Lett 2007, 246 (1-2), 262-7.

47. Lv, T.; Zhao, Y.; Jiang, X.; Yuan, H.; Wang, H.; Cui, X.; Xu, J.; Zhao, J.; Wang, J., uPAR: An Essential Factor for Tumor Development. J Cancer 2021, 12 (23), 7026-7040.

48. Ossowski, L.; Clunie, G.; Masucci, M. T.; Blasi, F., In vivo paracrine interaction between urokinase and its receptor: effect on tumor cell invasion. J Cell Biol 1991, 115 (4), 1107-12.

49. Smith, H. W.; Marshall, C. J., Regulation of cell signalling by uPAR. Nat Rev Mol Cell Biol 2010, 11 (1), 23-36.

50. Tjwa, M.; Sidenius, N.; Moura, R.; Jansen, S.; Theunissen, K.; Andolfo, A.; De Mol, M.; Dewerchin, M.; Moons, L.; Blasi, F.; Verfaillie, C.; Carmeliet, P., Membrane-anchored uPAR regulates the proliferation, marrow pool size, engraftment, and mobilization of mouse hematopoietic stem/progenitor cells. J Clin Invest 2009, 119 (4), 1008-18.

51. Yang, J. L.; Seetoo, D.; Wang, Y.; Ranson, M.; Berney, C. R.; Ham, J. M.; Russell, P. J.; Crowe, P. J., Urokinase-type plasminogen activator and its receptor in colorectal cancer: independent prognostic factors of metastasis and cancer-specific survival and potential therapeutic targets. Int J Cancer 2000, 89 (5), 431-9.

52. Hildenbrand, R.; Wolf, G.; Bohme, B.; Bleyl, U.; Steinborn, A., Urokinase plasminogen activator receptor (CD87) expression of tumor-associated macrophages in ductal carcinoma in situ, breast cancer, and resident macrophages of normal breast tissue. J Leukoc Biol 1999, 66 (1), 40-9.

53. Kim, S. J.; Shiba, E.; Taguchi, T.; Watanabe, T.; Tanji, Y.; Kimoto, Y.; Izukura, M.; Takai, S. I., Urokinase type plasminogen activator receptor is a novel prognostic factor in breast cancer. Anticancer Res 1997, 17 (2B), 1373-8.

VITA

Hsin-Yin Chuang was born in Taipei, Taiwan on January 15th, 1998. She graduated from National Taiwan Normal University (NTNU) in June 2020 with a Bachelor's degree in Life Science. She completed her first Master's degree in Life Science from NTNU in June 2021. She received her second Master's degree in Biological Sciences from Missouri University of Science and Technology in December 2023.